PROCEEDINGS OF THE ROYAL SOCIETY A MATHEMATICAL, PHYSICAL & ENGINEERING SCIENCES

The Mechanical Properties of Natural Materials. II. Microstructures for Mechanical Efficiency

L. J. Gibson, M. F. Ashby, G. N. Karam, U. Wegst and H. R. Shercliff

Proc. R. Soc. Lond. A 1995 **450**, 141-162
doi: 10.1098/rspa.1995.0076

The mechanical properties of natural materials. II. Microstructures for mechanical efficiency

By L. J. Gibson[1], M. F. Ashby[2], G. N. Karam[1], U. Wegst[2] and H. R. Shercliff[2]

[1]*Department of Civil and Environmental Engineering, Massachusetts Institute of Technology, Cambridge, MA 02139, USA*

[2]*Cambridge University Engineering Department, Trumpington Street, Cambridge CB2 1PZ, UK*

Many natural materials have exceptionally high values of the mechanical performance indices described in the previous, companion paper. For beams and plates of a given stiffness or strength, or for a column of a given buckling resistance, woods, palms and bamboo are among the most efficient materials available. Their mechanical efficiency arises from their combination of composite and cellular microstructures. In this paper we analyse the microstructures which give rise to exceptional performance, describe the fabrication and testing of model materials with those microstructures and discuss the implications for design of mechanically efficient engineering materials.

1. Introduction

Woods and palms are among the most efficient materials available for beams of a given stiffness or strength, or for columns of a given buckling resistance. As observed in the previous, companion paper (Ashby *et al.* 1995), they have values of the performance indices $E^{1/2}/\rho$, $E^{1/3}/\rho$, ${\sigma_f}^{2/3}/\rho$ and ${\sigma_f}^{1/2}/\rho$ equal or greater than those of virtually all engineering materials. Silk and muscle perform well as springs; skin is an excellent material for elastic hinges; and antler and nacre are an order of magnitude tougher than any engineering ceramic.

The natural function of each of these materials exploits their exceptional properties. Woods and palms resist bending (of the trunk from wind loads, or of branches from their own weight) and buckling (of the trunk). Silk stores elastic strain energy as an insect flies into, and is trapped by, the spider's web. Muscle stores and then releases elastic strain energy during locomotion. Antlers must be tough to withstand the rigours of rutting.

In this paper, we examine the role that microstructure plays in the mechanical efficiency of natural cellular materials. We focus on the elastic behaviour, but note that similar arguments could be made for other properties, such as strength. We first examine wood, one of the natural materials identified in the previous, companion paper. Both the composite nature of the cell wall and the cellular structure are modelled; both contribute to the efficiency. The results suggest that mechanical efficiency can be improved by reducing the relative density; the

Proc. R. Soc. Lond. A (1995) **450**, 141–162
Printed in Great Britain

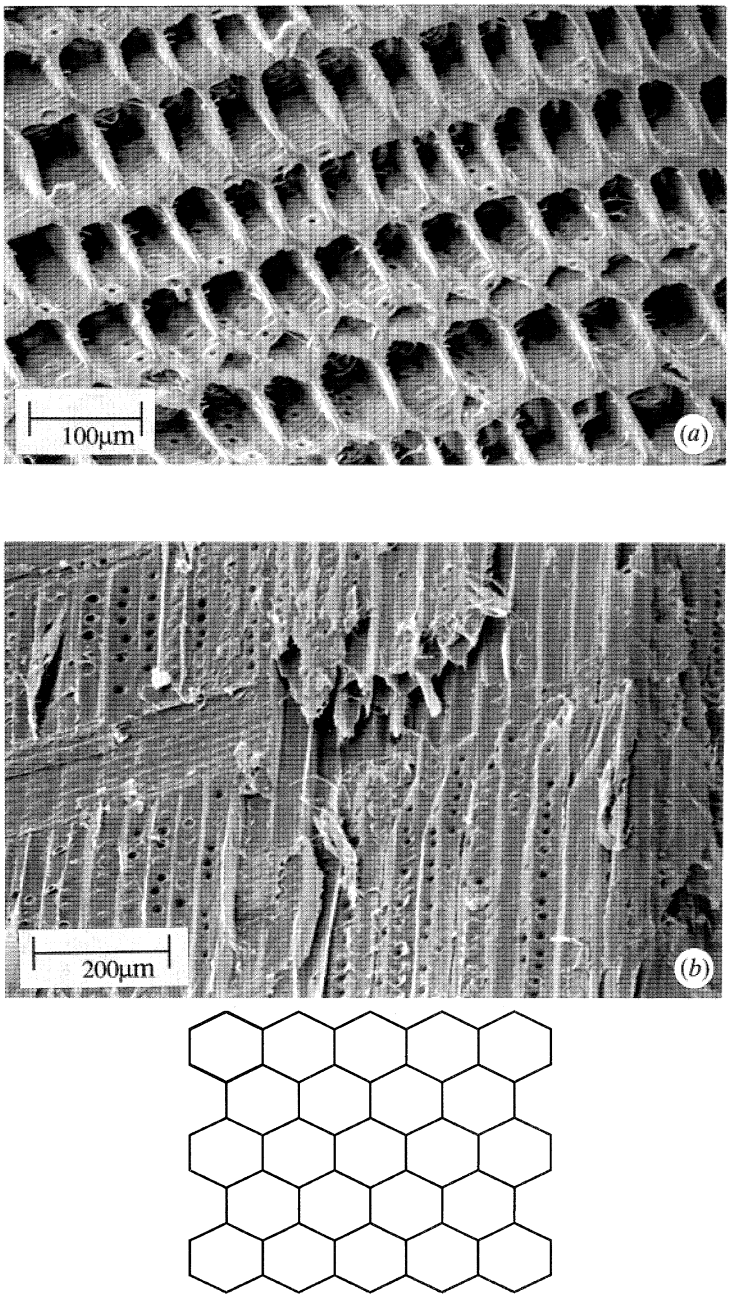

Figure 1. Scanning electron micrographs of Norway spruce (*Picea abies*): (*a*) cross-section and (*b*) longitudinal section;(*c*) schematic of wood structure, idealizing as a honeycomb-like array of hexagonal cells.

lower limit on relative density is determined by local buckling. We next examine palm and bamboo, which have fibrous bundles running longitudinally through a honeycomb-like matrix. In addition, bamboo has regularly spaced transverse discs known as septa where the leaves branch off from the stem. Finally we examine natural materials with microstructures resistant to local buckling: quills

and plant stems. Both have a thin, almost fully dense outer cylindrical shell with a cellular inner core. The results of the analysis suggest novel microstructures for mechanically efficient engineering materials for bending stiffness and elastic buckling resistance.

2. Woods

(*a*) *Structure*

The dominant feature of wood structure is the elongated cells visible in figure 1*a*, *b*. These tracheids, in softwoods, or fibres in hardwoods, provide the mechanical support for the tree. Both softwoods and hardwoods also have a small volume fraction (around 10%) of rays, made up of parenchyma cells which store food. Fluid conduction in softwoods is through the tracheids, while in hardwoods it is through vessels (Dinwoodie 1981; Bodig & Jayne 1982). As the height of the tree increases wood also grows radially, by cell division in the cambium at the interior of the bark; differences in growth rates with seasons produce the well known growth rings. We idealize the cellular structure by modelling only the tracheids or fibres as a honeycomb, as shown in figure 1*c*.

The cell-wall is a composite of cellulose fibres (or 'fibrils') in a matrix of lignin and hemicellulose. The orientation of the fibres is complicated: in general, the fibres lie more nearly parallel to the axis of the cell than normal to it. Knowing the layup, the Young's modulus for the cell wall can be calculated from composite theory (Mark 1967). For our purposes, it is easier to think of bounds within which the moduli must lie. They are constructed in figure 2, using the method of Ashby (1993); all dense composites of cellulose and lignin/hemi-cellulose have moduli which lie within the bound-envelope. The measured moduli of the wood cell wall, also shown on the figure, confirm this.

(*b*) *Modelling*

The grain of the wood lies parallel to the axis of the cells. When hollow prismatic cells are loaded parallel to the prism axis, the cell wall deforms uniaxially, either by stretching or compressing (Gibson & Ashby 1988); then the modulus is that of the cell wall in that direction, $E_{\mathrm{s,par}}$, reduced by the factor ρ/ρ_{s} where ρ is the overall wood density and ρ_{s} is that of the solid cell wall:

$$E_{\mathrm{par}} = E_{\mathrm{s,par}}\,(\rho/\rho_{\mathrm{s}})\,. \tag{1}$$

The density, for obvious reasons, also decreases as ρ/ρ_{s}, so the E–ρ trajectory for woods lies on a line of slope 1 on figure 2. The data (upper bubble) show that this is so; extrapolating the data to full density gives the cell-wall modulus parallel to the cell axis.

Loading across the grain causes the cell walls to bend rather than extend or compress uniaxially, giving a modulus in transverse direction of (Gibson & Ashby 1988):

$$E_{\mathrm{perp}} = E_{\mathrm{s,perp}}\,(\rho/\rho_{\mathrm{s}})^3\,, \tag{2}$$

where $E_{\mathrm{s,perp}}$ is the Young's modulus of the cell wall transverse to the grain. The data plotted on the figure (lower bubble) confirm this, and extrapolate to give the transverse modulus of the cell-wall; it is lower than the longitudinal modulus, as expected.

The cellular structure can enhance performance for loading parallel to the grain.

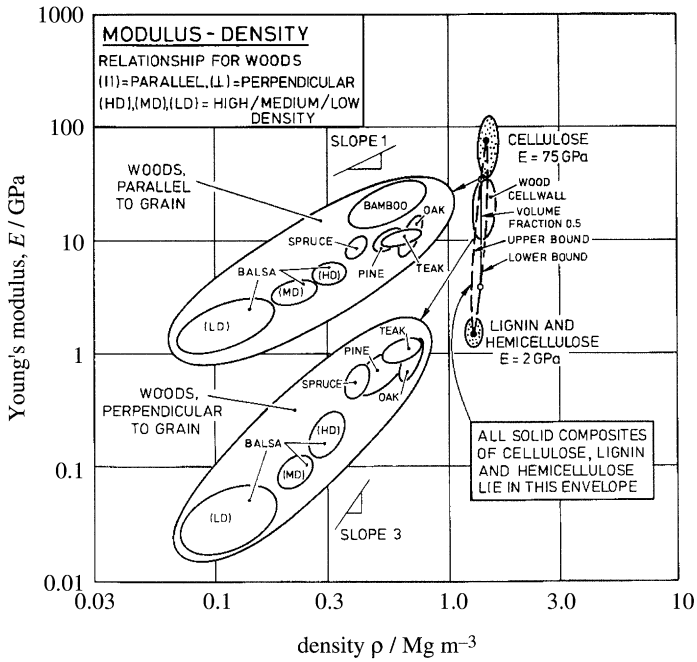

Figure 2. Material property chart plotting Young's modulus, E, against density, ρ, for woods and their constituents. The modulus of the wood cell wall lies between the upper and lower bounds calculated using a simple mechanics of materials approach. The data for woods loaded parallel to the grain lie along a line of slope 1.

We define the *relative efficiency* , ξ, of a cellular material as its performance index divided by that of the solid of which it is made†. Thus, using (1), we find the efficiency in axial tension parallel to the grain to be:

$$\xi_1 = \frac{M_1}{(M_1)_s} = \frac{E_{par}}{\rho} \Big/ \frac{E_{s,par}}{\rho_s} = 1, \tag{3}$$

where the subscript s means 'solid'. Here there is no gain in performance. But for bending of a beam cut with its longitudinal axis parallel to the grain

$$\xi_2 = \frac{M_2}{(M_2)_s} = \frac{E_{par}^{1/2}}{\rho} \Big/ \frac{E_{s,par}^{1/2}}{\rho_s} = \left(\frac{\rho_s}{\rho}\right)^{1/2}. \tag{4}$$

Here the performance gain is considerable. A balsa wood with a relative density of 0.1 has a relative efficiency in bending of 3: for a given bending stiffness, a balsa beam has $\frac{1}{3}$ the mass of a beam made from the solid cell wall material.

The relative efficiency for a plate bending stiffness appears to be larger still:

$$\xi_3 = \left(\frac{\rho_s}{\rho}\right)^{2/3}. \tag{5}$$

But this reflects only the high stiffness of the wood along the grain, parallel to the longitudinal axes of the cells. The lower transverse moduli of woods reduce

† A prismatic cellular tie, beam, column or plate with a value of $\xi = 2$ weighs less by this factor, than a solid one of the same stiffness or strength.

their efficiency for plate bending stiffness. Quasi-isotropic plates can be produced by laminating plies of wood with orientations of 0°, ±45° and 90°; plywoods are made with 0° and 90° plies. We can estimate the efficiency factor of plywood by noting that it is a symmetric cross-ply plate with roughly equal volume fractions of 0° and 90° plies giving an in-plane modulus of roughly:

$$E_{\text{in-plane}} = 0.5E_{\text{par}} + 0.5E_{\text{perp}}$$

or, using (1) and (2) and noting that the transverse modulus is negligible compared to the longitudinal modulus:

$$E_{\text{in-plane}} = 0.5E_{\text{s,par}}\,(\rho/\rho_{\text{s}})\,. \tag{6}$$

The efficiency factor ξ_3 then becomes:

$$\xi_3 = 0.8\,(\rho_{\text{s}}/\rho)^{2/3}\,. \tag{7}$$

For a plywood made from softwood with a relative density of 0.3, we estimate the efficiency factor ξ_3 to be 1.8. Data indicate that the efficiency factor for commercially available plywoods is about 2.0.

(*c*) *Model materials*

The mechanical efficiency of wood in bending stiffness arises from its microstructure of aligned prismatic cells. We have made model engineering materials ('honeycomb beams' and 'honeycomb plates') which exploit this microstructure (Huang & Gibson 1995). Square cross-sectioned honeycomb beams were made by casting an epoxy resin into a mould through which a 5 × 5 grid of parallel rubber tubes was strung; as is shown in the appendix, the 5 × 5 grid of 'cells' is sufficiently large to allow the material to be considered a continuum. After the epoxy had cured, the rubber tubes were removed, leaving a material with an array of parallel, cylindrical voids. The honeycomb beams were loaded in three-point bending and their Young's moduli were calculated from the slopes of the linear load–deflection curves. The efficiency factor, ξ_2 is compared with (5) in figure 3. A single honeycomb plate ($\rho/\rho_{\text{s}} = 0.59$) was made in a similar manner, with the tubes arranged in 0°/90°/0°/90°/90°/0°/90°/0° plies. The honeycomb plate was simply supported on all four edges and loaded at the centre; again, the Young's modulus was calculated from the slope of the load-deflection curve. The measured efficiency factor ξ_3 for the plate was 1.23 as compared with the value of 1.14 given by (7). The data for both efficiency factors are well described by the simple models of the previous section.

(*d*) *Implications for engineering design*

These results suggest that honeycomb beams and plates are efficient microstructures for bending stiffness. Two processes have recently been developed to produce such honeycomb microstructures commercially. Fibre composite honeycombs can be made by weaving the fibres into tubes, drawing the tubes over a mandrel, curing them to form individual rigid tubes, packing them to form a honeycomb and then curing them again, at a higher temperature, to bond the honeycomb together. Fibre composite honeycombs have been made with glass, carbon and Kevlar fibres by Courtaulds (D. Williams 1991, personal communication). Metal honeycombs can be made by dissolving a gas (usually hydrogen) into

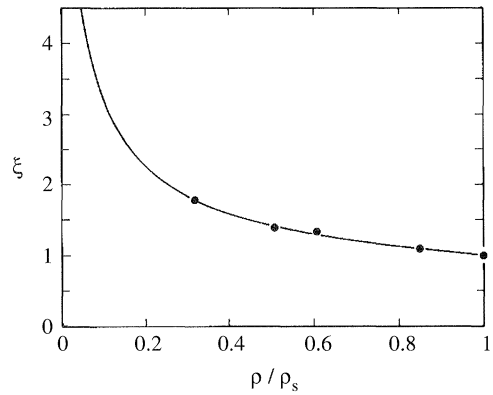

Figure 3. The efficiency factor ξ_2 for honeycomb beams plotted against relative density (from Huang & Gibson 1995).

a molten metal (e.g. copper, aluminum, iron, cobalt, or magnesium) and directionally cooling through the eutectic (Walukas 1992). Honeycomb materials with cell sizes ranging from 5 μm to 10 mm have been made by use of this process.

The efficiency factor of honeycomb beams increases with decreasing relative density or decreasing wall thickness to length ratio. The reduction in relative density is limited by the onset of local buckling. In § 4 we examine efficient microstructures for resisting local buckling.

3. Palm and bamboo

(*a*) *Structure*

Micrographs of sections through a palm petiole are shown in figure 4. The most striking feature of the structure are the relatively dense, fibre-like vascular bundles distributed throughout a 'matrix' of parenchyma cells. The longitudinal section (figure 4*c*) reveals that fibres and the honeycomb-like parenchyma cells are aligned with the longitudinal axis of the petiole. The distribution of the vascular bundles is radially uniform, allowing the petiole cross-section to be treated as a continuum.

Palm stems, on the other hand, have a non-uniform radial distribution of vascular bundles, with more bundles of larger diameter at the periphery than at the centre (Rich 1987). And unlike wood, palm lacks a cambium through which radial growth can occur to provide support with increasing height. Instead, palm stems rely largely on increasing the thickness and degree of lignification of older cell walls, leading to radial and longitudinal gradients in tissue density (figure 5, after Rich 1986, 1987).

The structure of bamboo is shown in the micrographs in figure 6. The stem is hollow and, like the palm, the stem wall has a radially varying volume fraction of 'fibres', increasing its flexural rigidity.

(*b*) *Modelling*

The palm petiole and stem suggest two models for mechanically efficient materials. The petiole is modelled as a unidirectional fibre composite with a uniform

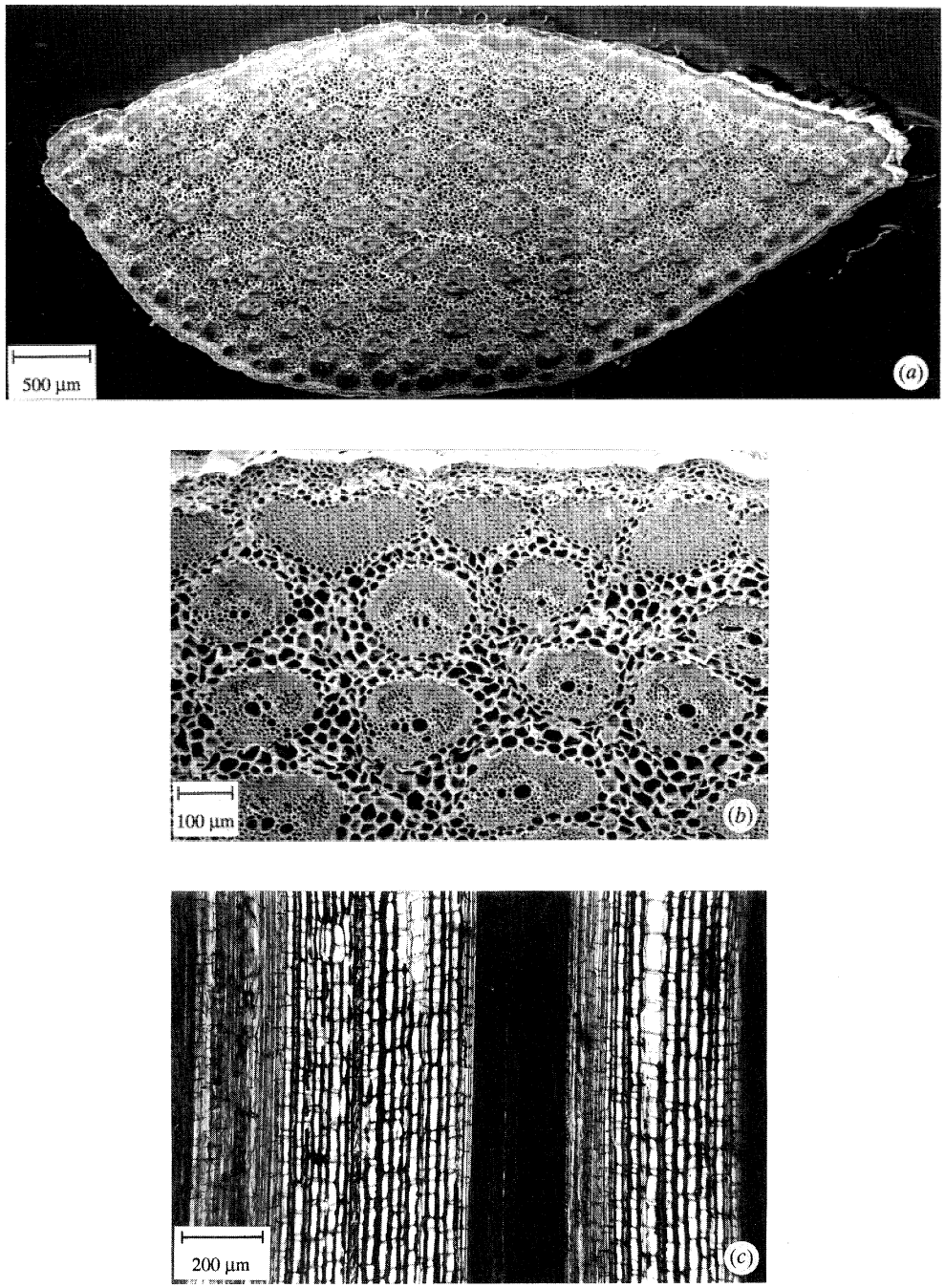

Figure 4. (*a*) Micrograph of a cross-section of a palm (*Chamaerops humilis*) petiole showing the uniform distribution of vascular bundles and parenchyma cells; (*b*) the same at higher magnification; (*c*) longitudinal section, showing the alignment of the vascular bundles and parenchyma.

distribution of fibres in a honeycomb matrix. We take the fibres to be made of the same solid material as the honeycomb matrix. The palm stem is modelled as a fibre composite with a radially varying volume fraction of fibres (figure 7).

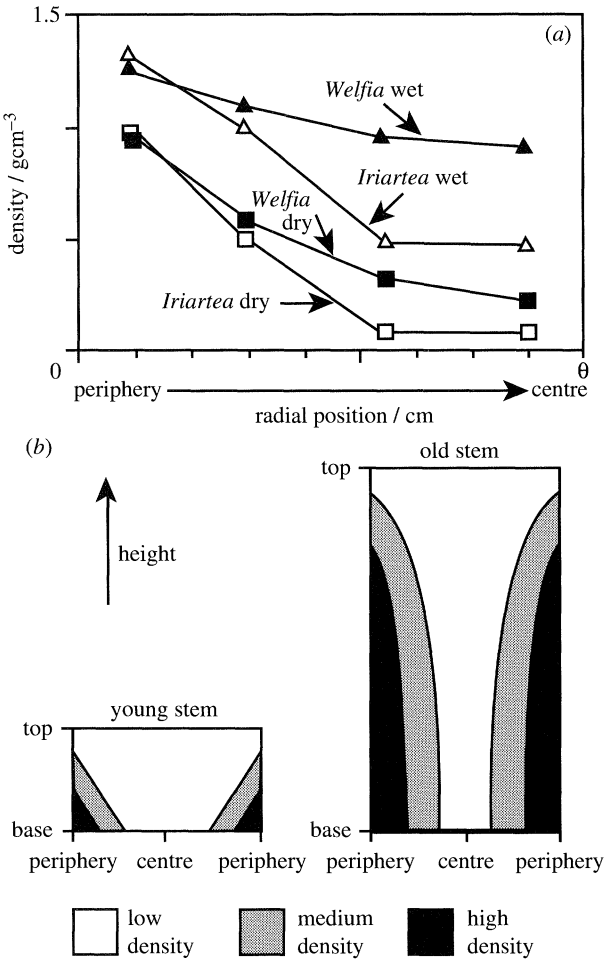

Figure 5. (*a*) Radial distribution of stem tissue density in a cross section at breast height within a 19 m tall *Welfia georgii* and within a 17 m tall *Iriartea gigantea* (after Rich 1987); (*b*) schematic representation of distribution of stem tissue dry density within a young palm stem (left) and an old palm stem (right) (after Rich 1987).

(i) *Uniform distribution of fibres*

The density of the composite is given by

$$\rho = f\rho_{\mathrm{f}} + (1 - f)\,\rho_{\mathrm{m}}, \tag{8}$$

where f is the volume fraction of fibres and ρ_{f} and ρ_{m} are the densities of the fibre and matrix, respectively. The Young's modulus in the direction of the fibres is given by

$$E = fE_{\mathrm{f}} + (1 - f)\,E_{\mathrm{f}}\,(\rho_{\mathrm{m}}/\rho_{\mathrm{f}})\,. \tag{9}$$

It is straightforward to calculate that the stiffness performance indices are then identical to those for woods, given by equations (3)–(5).

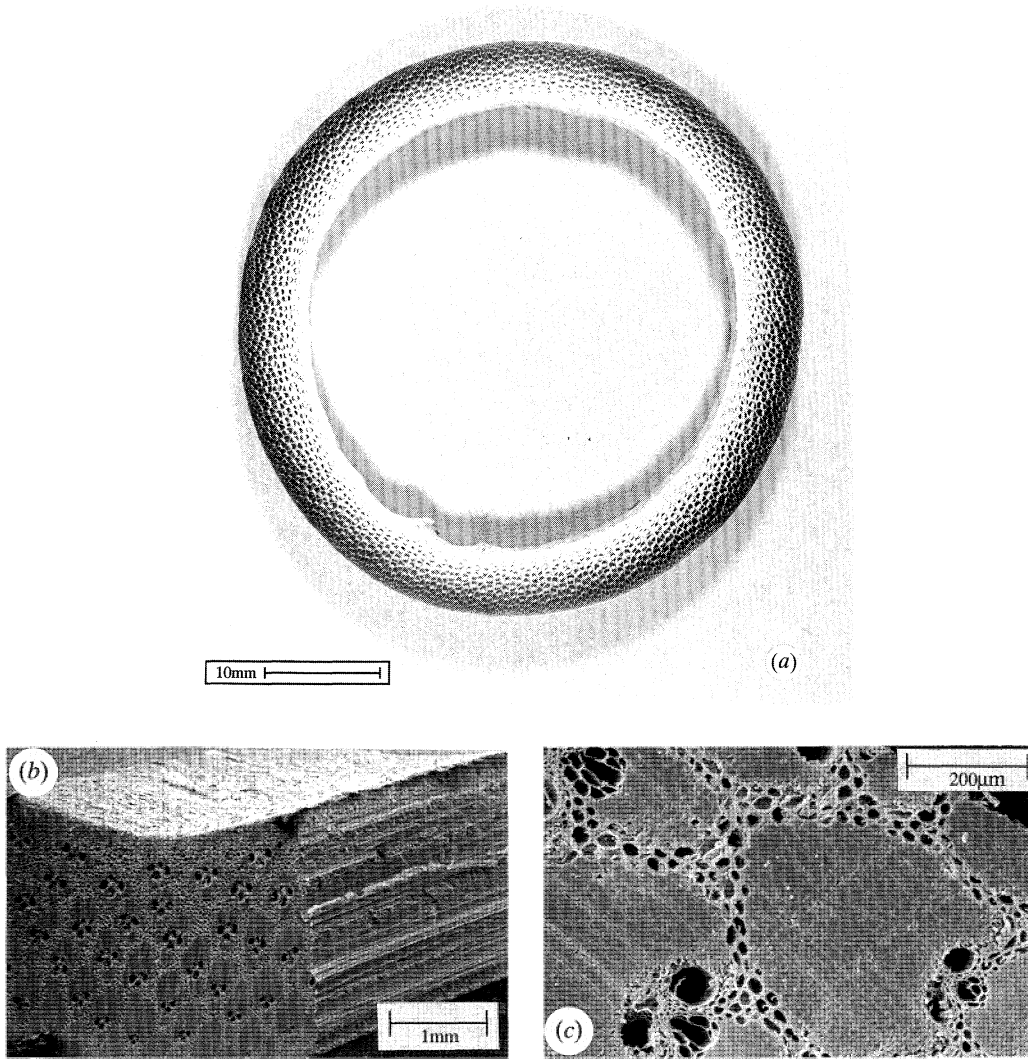

Figure 6. (*a*) Optical micrograph of a cross-section of a bamboo culm; (*b*) scanning electron micrograph of the wall of the bamboo culm showing the radial distribution of vascular bundles. The fibres and parenchyma are aligned with the longitudinal axis of the culm. The bundles have become almost totally sclerified in the tissue at the periphery. (*c*) Scanning electron micrograph of the vascular bundles at higher magnification.

(ii) *Radially varying volume fraction of fibres*

In palm, both the vascular bundles and the parenchyma cells are aligned in the longitudinal direction, giving a Young's modulus which varies linearly with density. As a consequence, a radial variation in the volume fraction of fibres is equivalent to a radial variation in the density of the cells. Here, we analyse a material with prismatic cells aligned in the longitudinal direction with a density varying radially from $\rho_{\min}$ at the centre to $\rho_{\max}$ at the periphery according to

$$(\rho - \rho_{\min})/(\rho_{\max} - \rho_{\min}) = (r/r_{\mathrm{o}})^{n}, \tag{10}$$

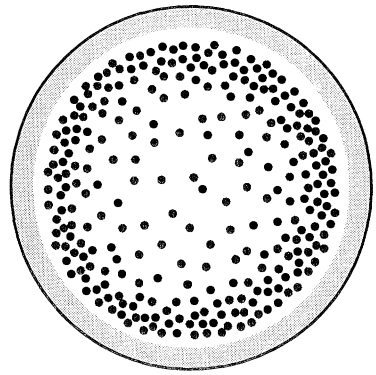

Figure 7. Schematic of a composite with a radially varying volume fraction of fibres producing a radial density gradient.

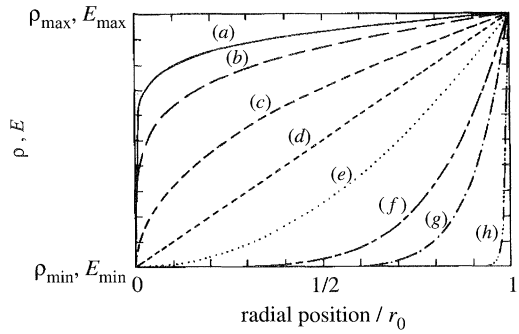

Figure 8. The dependence of the radial variation in density or Young's modulus on the parameter n (equation (10)): n = (*a*) 0.1, (*b*) 0.2, (*c*) 0.5, (*d*) 1, (*e*) 2, (*f*) 5, (*g*) 10, (*h*) 100.

where ρ is the density at a radius r and r_o is the outer radius (figure 8). The modulus of the composite material, E, depends on its density according to

$$E/E_s = \rho/\rho_s, \tag{11}$$

and we define R to be the ratio of the minimum (inner) to the maximum (outer) density:

$$R = \frac{\rho_{min}}{\rho_{max}} = \frac{E_{min}}{E_{max}}. \tag{12}$$

The average value of the density and of the modulus is then given by

$$\frac{\overline{E}}{E_{max}} = \frac{\overline{\rho}}{\rho_{max}} = \frac{1}{\pi r_o^2}\int_0^{r_o} \frac{\rho(r)}{\rho_{max}} 2\pi r \, dr = \frac{2+nR}{2+n}. \tag{13}$$

We next compare the performance of the composite with the radially varying density with that for a uniform solid section of density, $\overline{\rho}$, and Young's modulus, $\overline{E}$, in bending. Because the composite is not homogeneous, we cannot consider the performance in terms of the beam stiffness performance index, $E^{1/2}/\rho$. Instead, we compare the flexural rigidity, EI, of the composite section directly to that of a uniform circular section of equal mass. The flexural rigidity of a circular cross-section of the composite is (noting that the moment of inertia for a circular

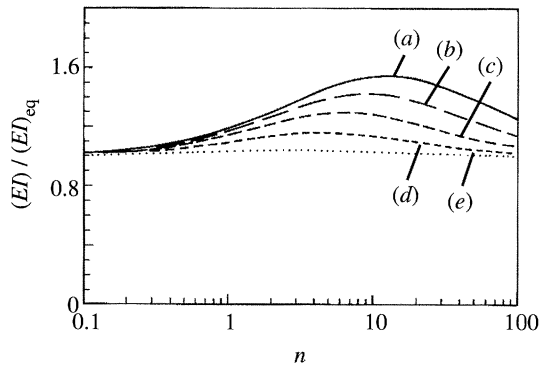

Figure 9. The flexural rigidity of a composite beam with a radial density gradient normalized by that of a solid circular cross-section of equal mass; $R =$ (*a*) 0.05, (*b*) 0.1, (*c*) 0.2, (*d*) 0.4, (*e*) 0.8.

cross section is one half of the polar moment of inertia):

$$(EI) = \tfrac{1}{2}\int_0^{r_o} E(r)2\pi r^3\,\mathrm{d}r$$
$$= \tfrac{1}{4}\pi r_o^4 \overline{E}\left[\frac{4(1-R)}{n+4} + R\right]\left(\frac{2+n}{2+nR}\right). \tag{14}$$

The flexural rigidity of the equivalent section is

$$(EI)_{eq} = \tfrac{1}{4}\pi r_o^4 \overline{E}. \tag{15}$$

The ratio of the flexural rigidities of the composite and uniform circular sections is then:

$$\frac{EI}{(EI)_{eq}} = \left[\frac{4(1-R)}{n+4} + R\right]\left(\frac{2+n}{2+nR}\right). \tag{16}$$

The ratio is plotted in figure 9. Data for the radial variation in density reported by Rich (1987*a*) suggest values of the density ratio, R, between 0.1 and 0.7 and of n between 0.3 and 1.6. A fibre-reinforced honeycomb matrix composite with a density gradient characterized by $n = 1.6$ and $R = 0.1$ has 1.24 times the flexural rigidity of the uniform material.

(*c*) *Model materials*

The effect of a distribution in fibre density was investigated experimentally. Rectangular beams, of approximate dimensions 10 mm×16 mm×240 mm, were cast in epoxy resin ($E = 1.11$ GPa), incorporating 9% volume fraction of stainless steel ($E = 195$ GPa) tubes of outer diameter 0.71 mm and wall thickness 0.15 mm as model hollow fibres. In one specimen, a homogeneous array of tubes was produced while in another, the tubes were concentrated towards the top and bottom surfaces, resembling a sandwich structure and giving a non-uniform distribution of fibres in the y direction (figure 10*a*, *b*). The measured axial Young's modulus of the homogenous specimen was 13.3 GPa while that of the inhomogeneous specimen was 13.0 GPa, in comparison with an expected value of 12.8 GPa.

The flexural rigidity of the two beams was measured in three point bending with the following results: $(EI) = 40.0\ \mathrm{Nm}^2$ for the homogeneous specimen and $(EI) = 58.3\ \mathrm{Nm}^2$ for the non-uniform specimen. The ratio of flexural rigidity of

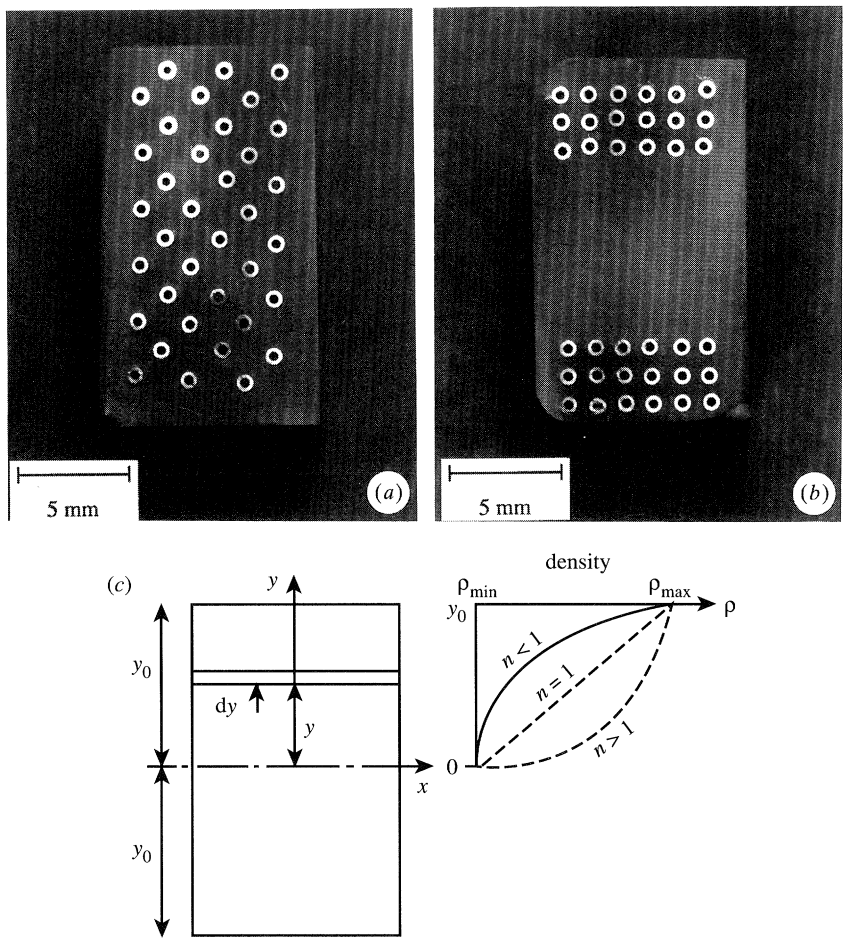

Figure 10. Model materials with stainless steel tubes in an epoxy matrix: (*a*) uniform distribution of tubes; (*b*) tubes distributed in the depth direction only; (*c*) schematic of a composite with a variation in the volume fraction of fibres in the depth direction $((\rho(y) - \rho_{\min})/(\rho_{\max} - \rho_{\min}) = (y/y_0)^n)$.

the non-uniform specimen to that of the homogeneous specimen is therefore 1.46. The gain in performance is simply due to the change in fibre distribution.

The analysis may be repeated for a rectangular beam of material with a density and modulus gradient in the depth or y-direction (figure 10*c*). The parallel expression for the ratio of flexural rigidities of a distributed and uniform section is then:

$$\frac{EI}{(EI)_{\text{eq}}} = \left[\frac{3(1-R)}{n+3} + R\right]\left(\frac{1+n}{1+nR}\right). \tag{17}$$

This ratio is plotted in figure 11. For the model material the middle half of the specimen has a constant modulus, $E_{\min}$=1.11 GPa, while the top and bottom quarters have a modulus of $E_{\max}$=24 GPa, giving $R = 0.04$. The discrete jump in modulus is best described by $n \sim 1$ (figure 8), giving an expected value of the

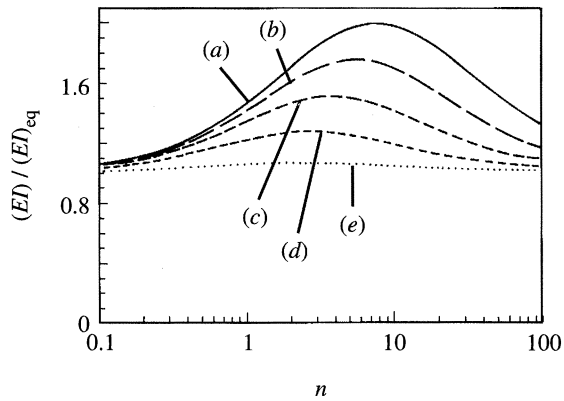

Figure 11. The flexural rigidity of a composite beam with a density gradient in the depth direction normalized by that of a composite with a uniform density distribution; $R =$ (*a*) 0.05, (*b*) 0.1, (*c*) 0.2, (*d*) 0.4, (*e*) 0.8.

ratio of the flexural rigidities, from (17), of 1.46, in excellent agreement with the data.

(*d*) *Implications for engineering design*

Varying the volume fraction of fibres radially in a fibre composite of circular cross-section leads to increased flexural rigidity over a uniform distribution. Further increases are possible if the cross-section is hollow, as in bamboo. Tubes are a standard part of the engineer's portfolio in designing stiff, light structures. Tubes with density and modulus gradients are not so standard. They have an advantage only when the tube wall has substantial thickness: a really thin-walled tube gains nothing from a structural gradient. There are some engineering examples. Composite tubes, particularly large diameter glass fibre reinforced cement tubes for drainage are made by spin casting. The glass is spun in first, concentrating it near the outer surface of the tube. The resulting property gradients enhance the performance of the tube.

4. Stems and quills

Plant stems resist both axial load (from their own mass) and bending moment (from wind loads): structurally, they act as beam-columns. Plant stems are axisymmetric, cylindrical tubes able to resist wind blowing from any direction equally. The shape factor, ϕ, gives a measure of the resistance of a cross-sectional shape to bending or Euler buckling. It is given by

$$\phi = 4\pi I/A^2, \tag{18}$$

where I is the second moment of area of the section and A is the cross-sectional area. The shape factor for a thin walled cylindrical tube is just the ratio of the radius to the wall thickness, a/t, suggesting that the most efficient cross-sectional shape is that with the largest radius and thinnest wall thickness. But this neglects local buckling. At high a/t ratios, the stem fails not by overall Euler buckling but by local buckling. Plant stems exploit at least two devices for suppressing local buckling: internal pressurization of the stem (e.g. chives) and support of a dense, stiff outer shell by an elastic foundation of foam-like material (e.g. grasses).

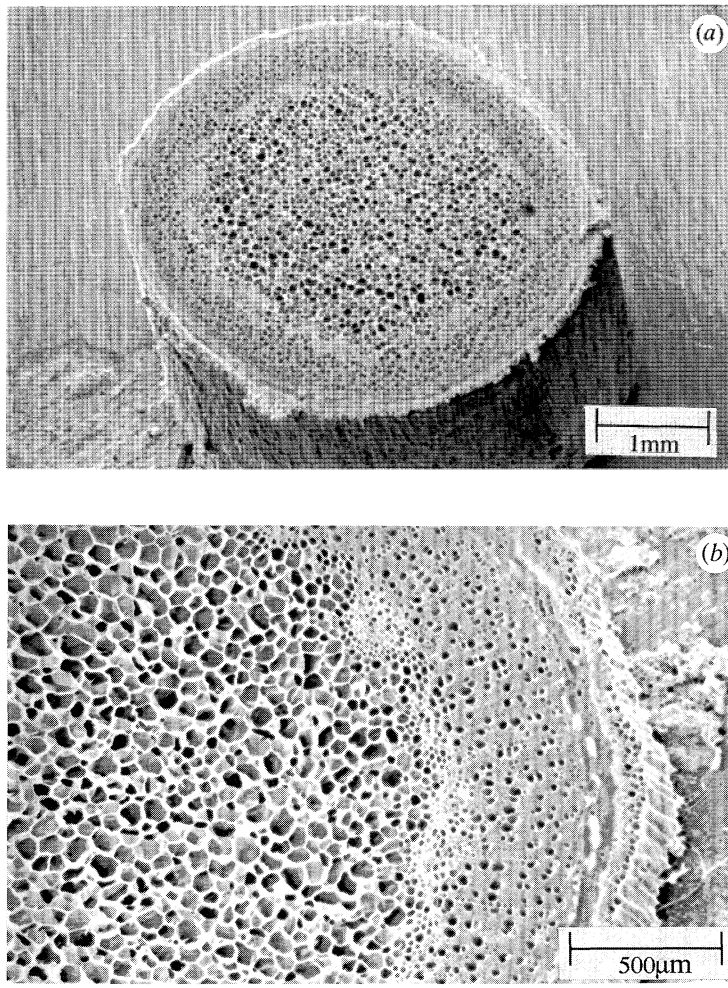

Figure 12. Scanning electron micrographs of hawthorn (*Craetagus*) showing the outer, almost fully dense, cylindrical shell with an inner layer of foam-like parenchyma cells.

Niklas & O'Rourke (1987) have described the contribution of internal pressure to flexural rigidity. Here we examine the increase in resistance to local buckling arising from the presence of a foam-like core.

(*a*) *Structure*

Many plant stems have an outer, almost fully dense, cylindrical shell lined with an inner layer of foam-like parenchyma cells. In some cases, the parenchyma completely fill the shell (figure 12*a*, *b*) while in others there is a central void. Examples of this structure can be found in barley (*Hordeum*), oat (*Avena*) and rye (*Secale*). Similar structures are also found in hedgehog spines and porcupine quills (Vincent & Owers 1986) (figure 13). We idealize the structure as a cylindrical shell of radius a, thickness t, density ρ, Young's modulus E, and Poisson's ratio ν, lined with a foam core of thickness c, density ρ_{f}, Young's modulus E_{f}, and Poisson's ratio ν_{f} (figure 14*a*).

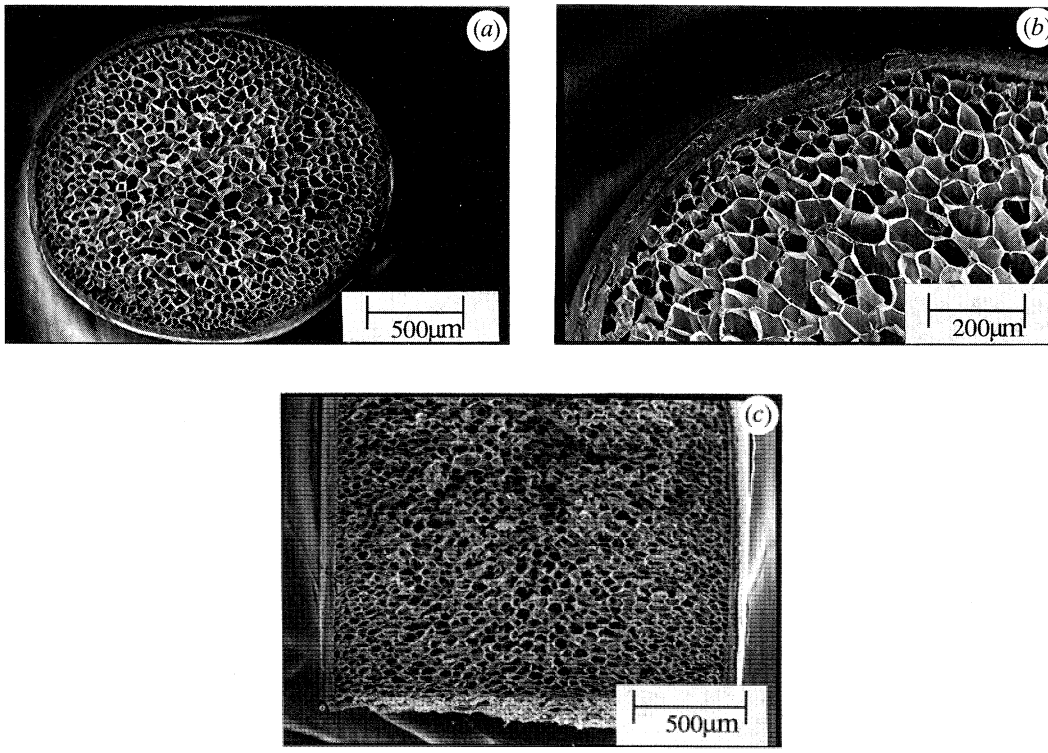

Figure 13. Scanning electron micrographs of porcupine (*Erethizon*) quills. (a, b) Transverse sections; (c) longitudinal section.

(*b*) *Modelling*

We have analysed the elastic stability of a cylindrical shell with a foam core subject to an axial load. The foam core acts as an elastic foundation, resisting bending of the shell. We have solved the two-dimensional elastic buckling problem by analysing a strip of the shell as shown in figure 14. The critical buckling load, $\sigma_{\rm cr}$, is found to be (Karam & Gibson 1995*a*):

$$\sigma_{\rm cr} = \sqrt{3(1-\nu^2)}\sigma_{\rm o} f_1, \tag{19}$$

where $\sigma_{\rm o}$, the buckling stress of an empty cylindrical shell under an axial load, is given by

$$\sigma_{\rm o} = \frac{Et}{a\sqrt{3(1-\nu^2)}}, \qquad f_1 = \frac{1}{12\,(1-\nu^2)}\frac{a/t}{(\lambda_{\rm cr}/t)^2} + \frac{(\lambda_{\rm cr}/t)^2}{a/t} + \alpha\frac{(\lambda_{\rm cr}/t)}{t/a},$$

and $\lambda_{\rm cr}$, the half buckled wavelength divided by π, is found from the solution to

$$\frac{-t^3}{12(1-\nu^2)\lambda^3} + \frac{t\lambda}{a^2} + \frac{E_{\rm f}/E}{(3-\nu_{\rm f})(1+\nu_{\rm f})} = 0. \tag{20}$$

We next analysed the case of a cylindrical shell with a foam core subject to a bending moment (Karam & Gibson 1995*a*). Hollow cylindrical shells ovalize under a bending moment: as the curvature increases, the cross-section gradually changes from circular to oval, reducing the second moment of area of the cross-

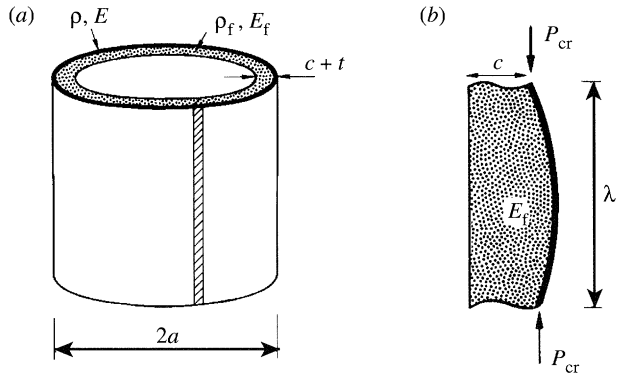

Figure 14. (*a*) Schematic drawing of cylindrical shell with an inner core of foam; (*b*) analysis of the shell and foam core as a two-dimensional strip.

section. The moment-resisting capacity of the tube reaches a maximum at the Brazier moment. True local buckling occurs when the compressive stress in the wall of the tube is equal to the buckling stress under uniaxial compression of the tube. In hollow tubes, local buckling occurs at slightly lower moments than the Brazier moment. In cylindrical tubes with a compliant core, the core acts in two ways: it resists ovalization of the cross-section and acts as an elastic foundation. We have calculated both the Brazier moment and the local buckling stress for a foam-filled cylindrical shell by minimizing strain energy; as in the case of the hollow shell, local buckling always precedes the Brazier moment. We have also calculated the decay in normal and shear stresses with radial distance into the core. At a depth of about 1.6 times the buckling half-wavelength the stresses decay to about 5% of their maximum values, suggesting that the innermost core resists little load and can be removed without significant reduction in moment carrying capacity.

Using the calculations described above we have compared the buckling resistance of a hollow cylindrical shell with that of a cylindrical shell with a compliant core of equal mass and radius. The foam-core shell is assumed to have the innermost part of the foam-core, which resists little load, removed. Plots of the buckling resistance of the hollow shell relative to that of the foam-core shell are shown in figure 15. Under uniaxial compression (figure 15*a*) the shell with the foam core has a higher resistance to buckling than the equivalent hollow shell for thin walled shells (high a/t) with relatively dense cores; in pure bending, the shell with the foam core has a higher buckling resistance than the hollow shell in every case.

(*c*) *Model materials*

Silicone rubber cylindrical shells with and without foam cores have been fabricated and tested in uniaxial compression and four point bending (Karam & Gibson 1995*b*). Typical test results are compared with the analysis in figure 16. In the uniaxial compression tests (figure 16*a*) the silicone rubber shells were first tested without any core ($c/t = 0$). They were then filled with a more compliant silicone rubber foam ($E_f/E = 0.1$) and retested ($c/t = a/t - \frac{1}{2}$). Filling the shell with the core led to dramatically increased buckling loads, but with large increases in weight. As the bulk of the core resists no load, we then removed

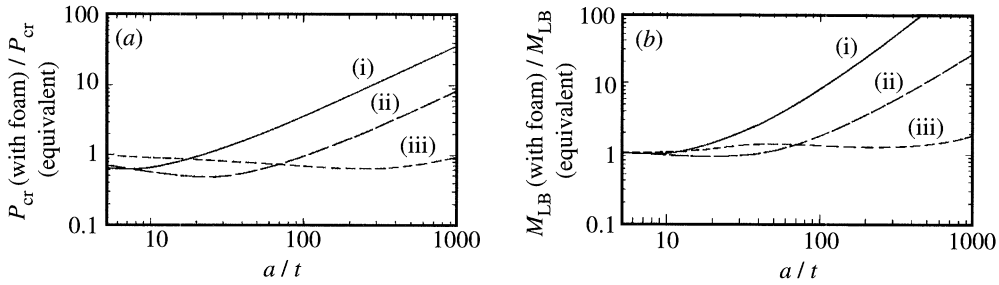

Figure 15. The buckling resistance of the foam core cylindrical shell to that of the hollow cylindrical shell at constant mass and radius (*a*) for uniaxial compression, (*b*) for bending. (i) $\rho_f/\rho = 0.3$, $E_f/E = 0.1$; (ii) $\rho_f/\rho = 0.1$, $E_f/E = 0.01$; (iii) $\rho_f/\rho = 0.01$, $E_f/E = 0.0001$. (After Karam & Gibson 1995*a*.)

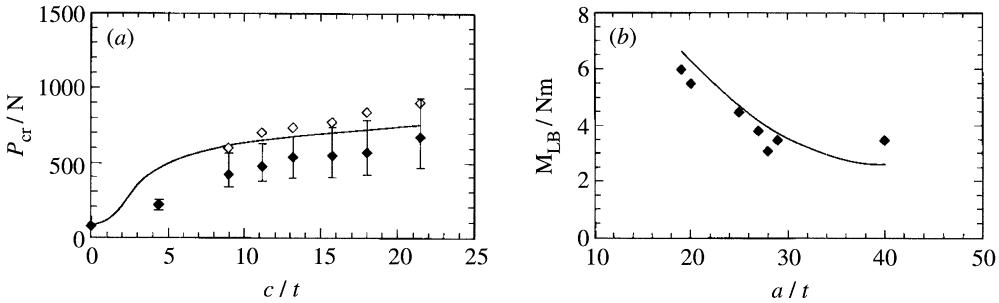

Figure 16. (*a*) The dependence of the critical buckling load of a cylindrical shell with the foam core in uniaxial compression on the ratio of the foam-core thickness to the cylindrical shell thickness, c/t. The solid line represents the theory; diamonds represent data from uniaxial compression tests on silicone rubber tubes with varying core thicknesses ($a/t = 22$; $E_f/E = 0.1$): ♦, experimental data; ◊, quasi-perfect specimen. (*b*) The critical buckling moment of silicone rubber beams with a polyurethane foam core plotted against the radius to shell thickness ratio, a/t ($\rho_c/\rho = 0.01$, $E_c/E = 0.01$). (After Karam & Gibson 1995*b*.)

increasing increments of foam from the centre of the core with a hole saw; the specimens were then retested, giving the points at intermediate c/t ratios. The filled diamonds represent specimens in which there was an initial imperfection caused by the specimen production technique; the open diamonds represent a specimen with almost no initial imperfection. The data confirm the analyses of both axisymmetric buckling and stress decay within the core. Four point bending tests were performed on approximately 890 mm long, 146 mm diameter silicone rubber shells lined with 25 mm of polyurethane foam ($E_f/E = 0.01$) (figure 16*b*). The analysis of local buckling describes the measured local buckling moment well. The agreement between the data and the analysis gives confidence in our comparisons of the buckling resistance of cylindrical shells with and without a compliant core (figure 15).

(*d*) *Implications for engineering design*

Engineers design structures ranging from aircraft fuselages to offshore oil jackets to missile silos as thin-walled cylindrical shells (figure 17). Such structures are currently reinforced against local buckling by welding circumferential and longitudinal stiffeners within the tube. The recently developed GASAR process (which

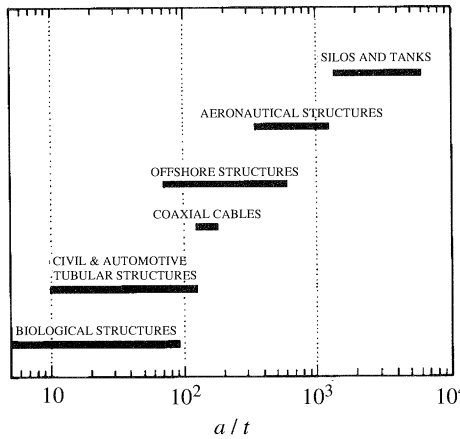

Figure 17. Values of a/t for typical engineering structures. (After Karam & Gibson 1995*a*.)

produces porous metals by cooling a molten metal/hydrogen gas mixture through the eutectic point) allows the manufacture of a cylindrical metal shell with a more compliant foamed metal core as a single unit. The results of this study suggest that such a structural component offers resistance to local buckling at reduced weight. The GASAR process has successfully been used to produce several metal foams including iron, aluminum, copper and nickel.

5. Conclusions

Many natural materials have anisotropic cellular structures which orient solid preferentially in the direction of loading. A beam made from them has a stiffness in bending which is greater than that of a solid beam of the same weight per unit length. We describe this gain in stiffness by the relative efficiency, ξ, of the structure. Wood, for instance, is made up of prismatic cells with the prism axis parallel to the longitudinal axis of the trunk or branch; simple modelling shows how this microstructure increases the bending stiffness, and thus the relative efficiency, as the density of the wood decreases. Palm has a more complex structure than wood, with a radial density gradient of parallel tubular fibres in a matrix of honeycomb-like cells, features which increase its flexural rigidity and relative efficiency. Bamboo increases the flexural rigidity even further by combining the radial density gradient with an efficient cross section, a hollow tube. Grasses and porcupine quills have a dense outer shell supported by a foam-like compliant core which acts to suppress failure by local buckling.

The performance of engineered materials can be improved by designing them to have structures described here. A few exist already; the others could, in principle, be made but will require the development of novel processing routes. It would appear worthwhile to pursue them.

We are grateful to Professor Pat Echlin of the Botany Department, Cambridge University for helpful discussions, to Doctor Peter Yeo and Mr. Spong of the Cambridge University Botanical Garden for generously supplying specimens of palms, and to Mr. Michael Lynch of the Franklin Park Zoo, Boston, MA and Mr. Tomasz Owerkowicz and Ms. M. Rutzmaser and T. McFadden of the Museum of Comparative Zoology, Harvard University for generously supplying hedgehog spines and porcupine quills. As always, Mr. Alan Heaver of the Cambridge University Engineer-

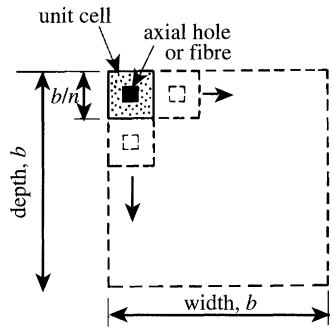

Figure 18. Schematic of model cross-section showing a unit cell with either a void or a fibre.

ing Department provided enthusiastic assistance with the microscopy and Mrs. Sheila Mason skillfully prepared the line drawings, for which we are grateful. The University of Chicago Press graciously gave permission to reproduce figure 5. Financial support for this project was provided by the US National Science Foundation (Grant No. MSS-9202202), the NATO Program for International Collaborative Scientific Research and the Royal Society, which provided a summer studentship for UGKW.

Appendix A. The effect of microstructural length scale on flexural rigidity

Many of the natural materials and model materials discussed in this paper have a composite microstructure, often with one or both of the components a cellular solid. If the microstructural length scales (e.g. cell size, fibre diameter and spacing) are small compared to the specimen size, then the flexural rigidity (EI) can be evaluated treating the material as a continuum. In particular, if the composite structure is homogeneous across the section, then the modulus in bending derived from (EI) is equal to the normal tensile modulus of the material, E. It has been shown by Ashby (1992) that a fine-scale cellular structure leads to improved performance in bending compared to the solid of which the cell walls are made – the material is then said to be 'microshaped'.

Examination of the structures of palm, for example, indicate that the length scale of the microstructure is not small compared to the diameter of the section – there are perhaps only 8–10 fibre bundles across the section. The question arises therefore as to whether such a microstructure can be classified as microshaped, i.e., behaving with the same apparent modulus in bending as in tension.

To investigate the effect of length scale, the flexural rigidity of two model sections have been evaluated. The first section comprises unit cells of solid matrix with a central square hole aligned along the axis of the beam; the second has a unit cell of solid matrix with a central square fibre, with a modulus greater than that of the matrix by a specified factor. In each case, the depth of the beam b is made up of n unit cells; the size of the unit cell is thus b/n (figure 18). For convenience, a square beam of $n \times n$ cells is considered, though the number of cells in the width direction is of no consequence. Note that as n varies, the volume fraction of matrix remains constant as all the dimensions of the unit cell scale proportionately – hence all that changes is the coarseness of the microstructure compared to the specimen dimensions. For a given n, the flexural rigidity is evaluated exactly, and then divided by the second moment of area of the section

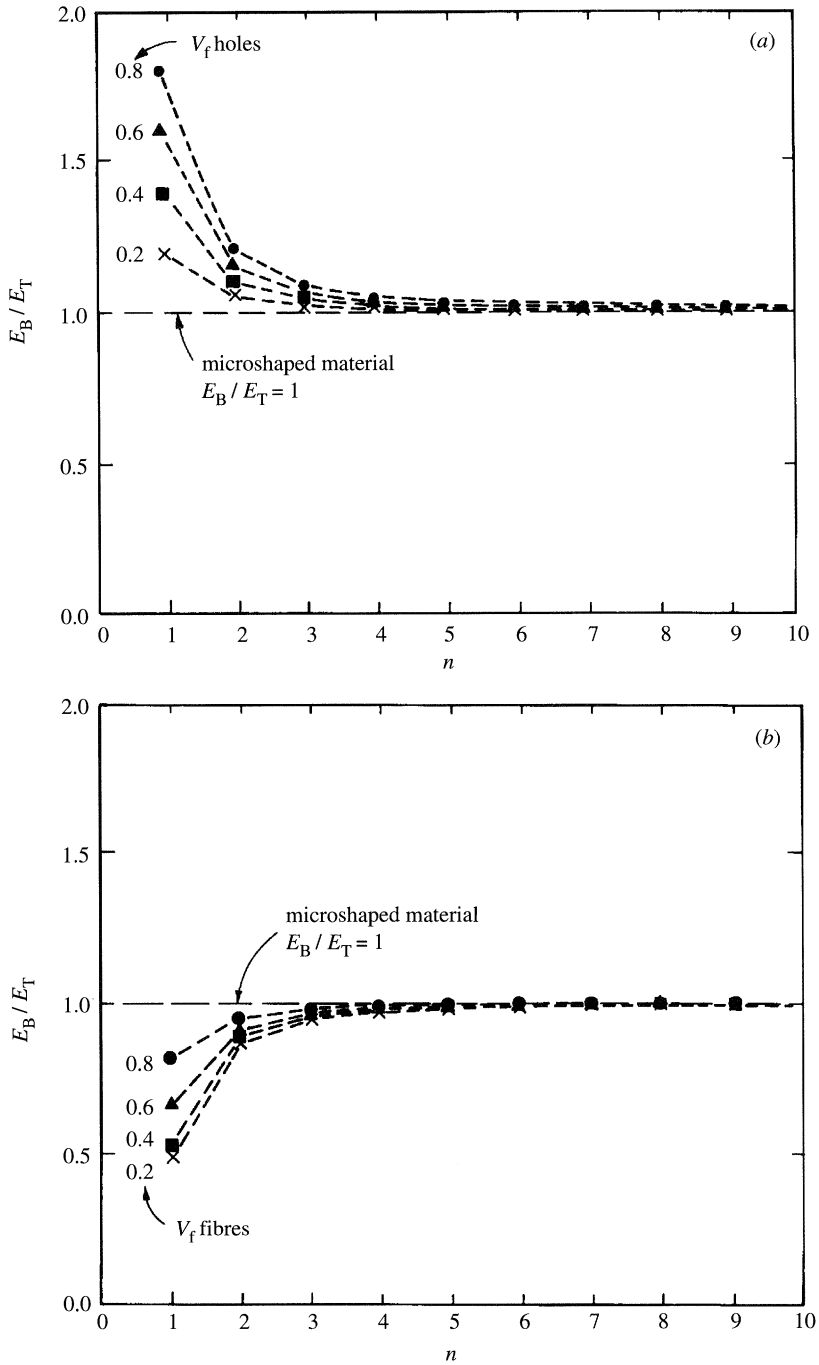

Figure 19. (*a*) Ratio of apparent modulus in bending to axial tensile modulus E_B/E_T for a cross section with a unit cell with a volume fraction V_f of voids plotted against number of cells n. The cross section behaves as a continuum at about $n = 4$; (*b*) ratio of apparent modulus in bending to axial tensile modulus E_B/E_T for a cross-section with a unit cell with a volume fraction V_f of fibres plotted against number of cells n. The ratio of fibre to matrix modulus is 10. The cross-section behaves as a continuum at about $n = 4$.

$I = b^4/12$ to give an apparent modulus in bending E_B. The axial tensile modulus, E_T in each case is calculated using the appropriate rule of mixtures. The ratio E_B/E_T is plotted for the two sections in figure 19, as a function of the number of unit cells across the depth, and for different volume fractions of holes in case (*a*) and fibres in case (*b*). The modulus ratio of fibres to matrix in case (*b*) is taken to be 10.

When the ratio E_B/E_T approaches unity, then the material can be treated as a continuum. It can be seen from figure 19*a* that a matrix containing axial holes is effectively microshaped once the number of unit cells is about 4 or more. The volume fraction of solid has only a secondary effect. The apparent modulus in bending is greater than the tensile modulus in all cases – in the limit of $n = 1$ it is clear that the bending performance will be improved, as this is simply removing material lying on the neutral axis, forming a hollow section. For the fibre composite in figure 19*b*, the material also effectively behaves as a continuum once there are about 4 unit cells across the depth, with again only a small effect of volume fraction. Here the limit of $n = 1$ is inefficient in bending as the stiff fibre lies on the neutral axis – so by increasing the number of cells, the continuum modulus is approached from below.

It is perhaps surprising that so few units of the microstructure are required before the material in bending can be treated as a continuum with average tensile properties. For the case of palm, we can therefore conclude that the fibre structure is fine enough to treat the material as a continuum. It is therefore valid to examine the improvement in rigidity achieved by having a gradient of density and modulus by considering a smooth gradient in properties. The results are not influenced by the apparent coarseness of the microstructure. Similarly, the layup of plates containing prismatic holes can be modelled as a material of reduced modulus and density once the number of layers exceeds about 4.

References

Ashby, M. F. 1992 *Materials Selection in Mechanical Design.* Oxford: Pergamon.

Ashby, M. F. 1993 Criteria for selecting the components of composites. *Acta metall. mater.* **41**, 1313–1335.

Ashby, M. F., Gibson, L. J., Wegst, U. & Olive, R. 1995 The mechanical properties of natural materials. I. Material property charts. *Proc. R. Soc. Lond.* A **450**, 123–140. (Previous paper.)

Bodig, J. & Jayne, B. A. 1983 *Mechanics of wood and wood composites.* New York: van Nostrand Reinhold.

Dinwoodie, J. 1981 *Timber: its structure and properties.* New York: van Nostrand Reinhold.

Gibson, L. J. & Ashby, M. F. 1988 *Cellular solids: structure and properties.* Pergamon.

Huang, J. S. & Gibson, L. J. 1995 Microstructural design of cellular materials. I. Honeycomb beams and plates. *Acta metall. mater.* **43**, 1643–1650.

Karam, G. N. & Gibson, L. J. 1995*a* Elastic buckling of cylindrical shells with elastic cores. I. Analysis. *Int. J. Sol. Struct.* **32**, 1259–1283.

Karam, G. N. & Gibson, L. J. 1995*b* Elastic buckling of cylindrical shells with elastic cores. II. Experiments. *Int. J. Sol. Struct.* **32**, 1285–1306.

Mark, R. E. 1967 *Cell wall mechanics of tracheids.* Princeton University Press.

Niklas, K. J. 1992 *Plant biomechanics: an engineering approach to plant form and function.* University of Chicago Press.

Niklas, K. J. & O'Rourke, T. D. 1987 Flexural rigidity of chive and its response to water potential. *Amer. J. Bot.* **74**, 1033–1044.

Rich, P. M. 1986 Mechanical architecture of arborescent rain forest palms. *Principes – J. Int. Palm Soc.* **30**, 117–131.

Rich, P. M. 1987 Mechanical structure of the stem of arborescent palms. *Bot. Gaz.* **148**, 42–50.

Vincent, J. F. V. & Owers, P. 1986 Mechanical design of hedgehog spines and porcupine quills. *J. Zool. Lond.* A **210**, 55–75.

Walukas, M. 1992 *GASAR materials: A novel approach in the fabrication of porous materials.* Ann Arbor, MI: USP Holdings.

Received 21 July 1994; revised 1 November 1994; accepted 9 November 1994

PROCEEDINGS OF THE ROYAL SOCIETY A MATHEMATICAL, PHYSICAL & ENGINEERING SCIENCES

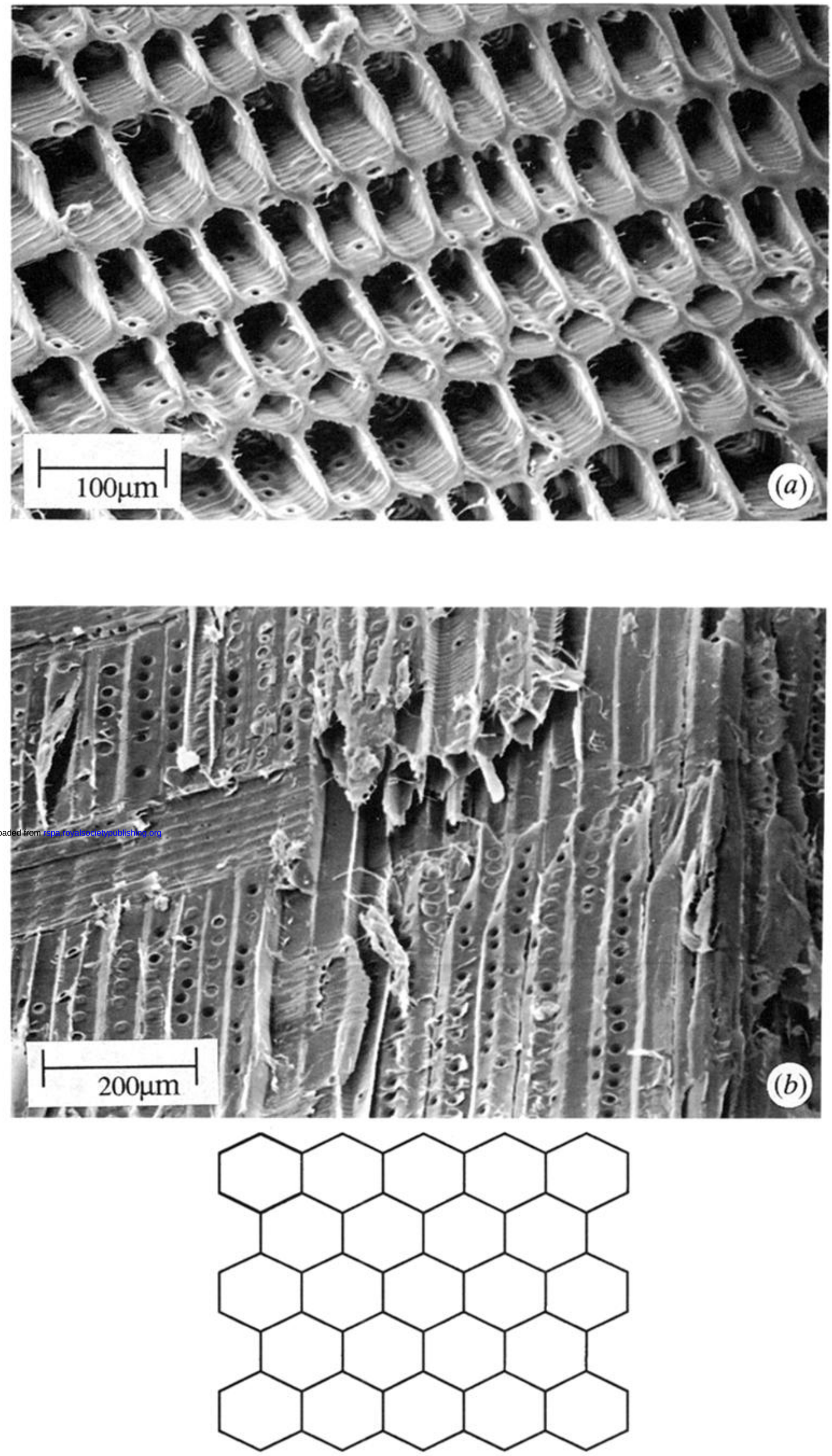

igure 1. Scanning electron micrographs of Norway spruce (*Picea abies*): (*a*) cross-section and) longitudinal section;(*c*) schematic of wood structure, idealizing as a honeycomb-like array of exagonal cells.

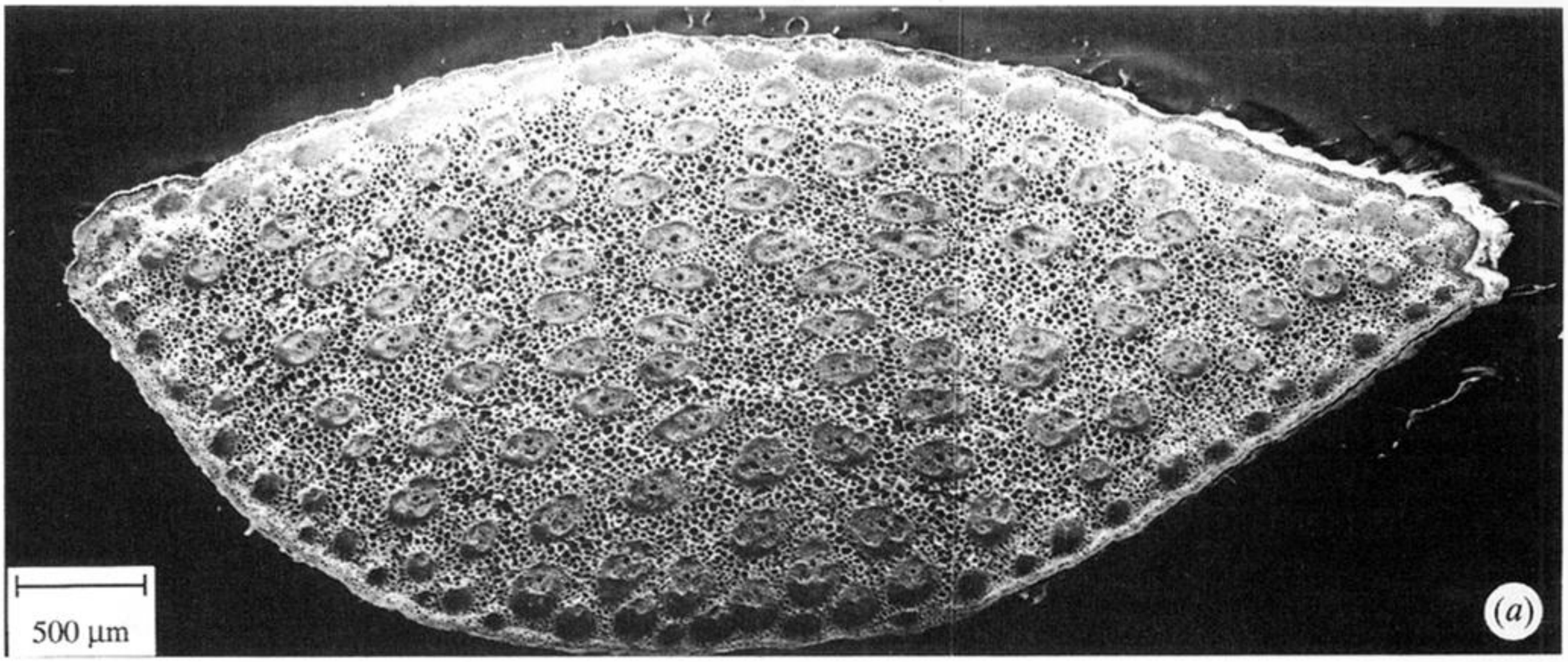

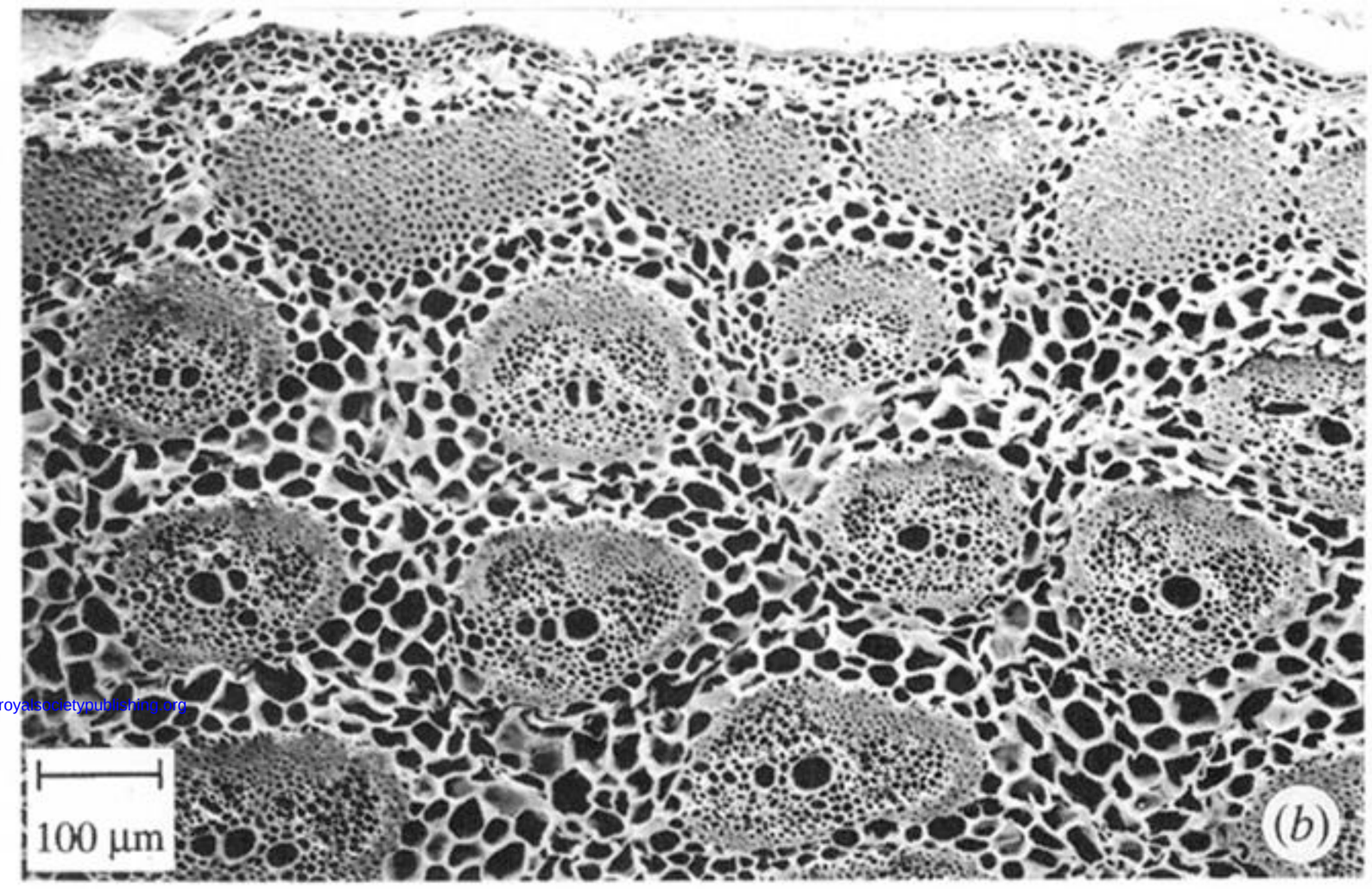

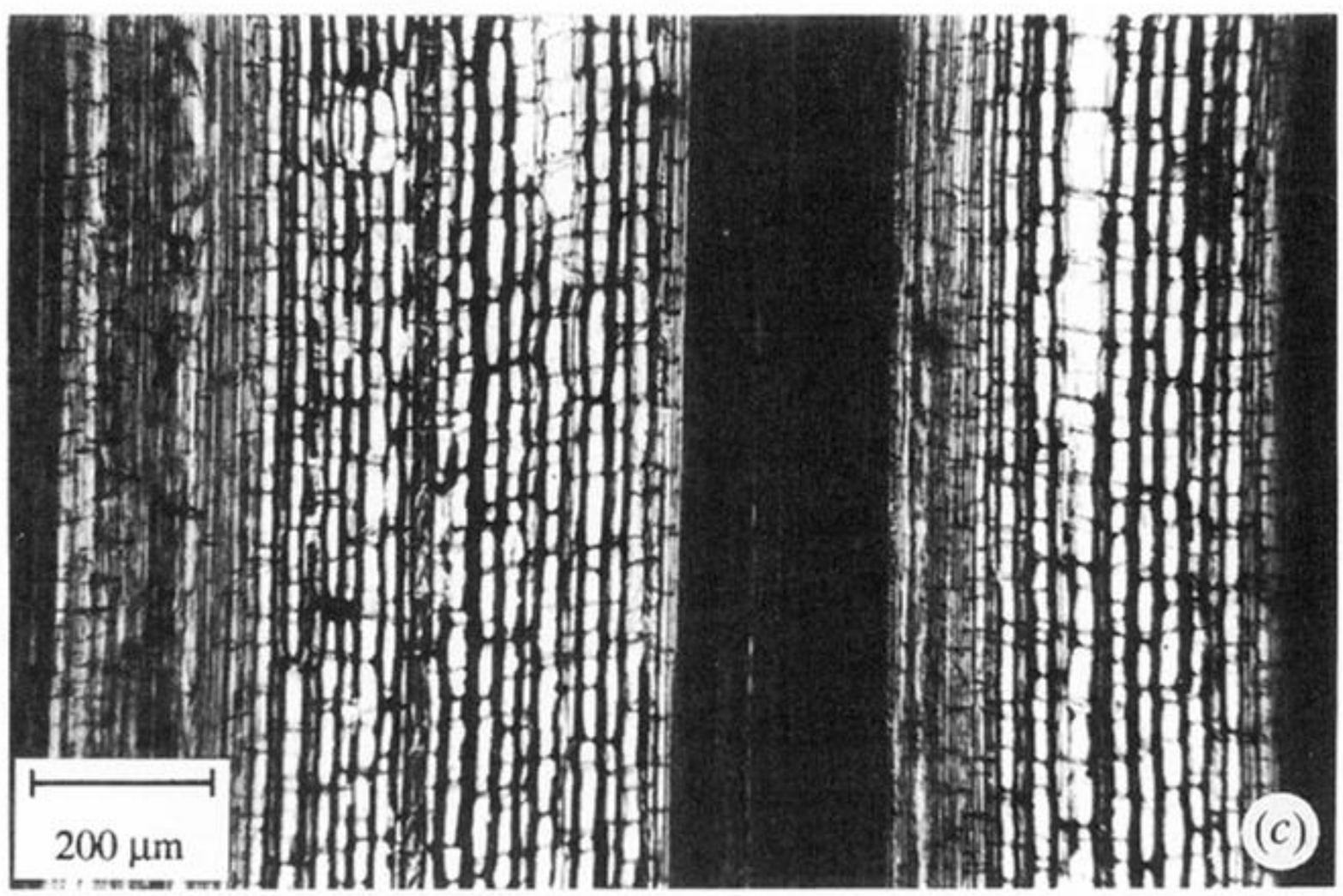

igure 4. (*a*) Micrograph of a cross-section of a palm (*Chamaerops humilis*) petiole showing the niform distribution of vascular bundles and parenchyma cells; (*b*) the same at higher magnifi- tion; (*c*) longitudinal section, showing the alignment of the vascular bundles and parenchyma.

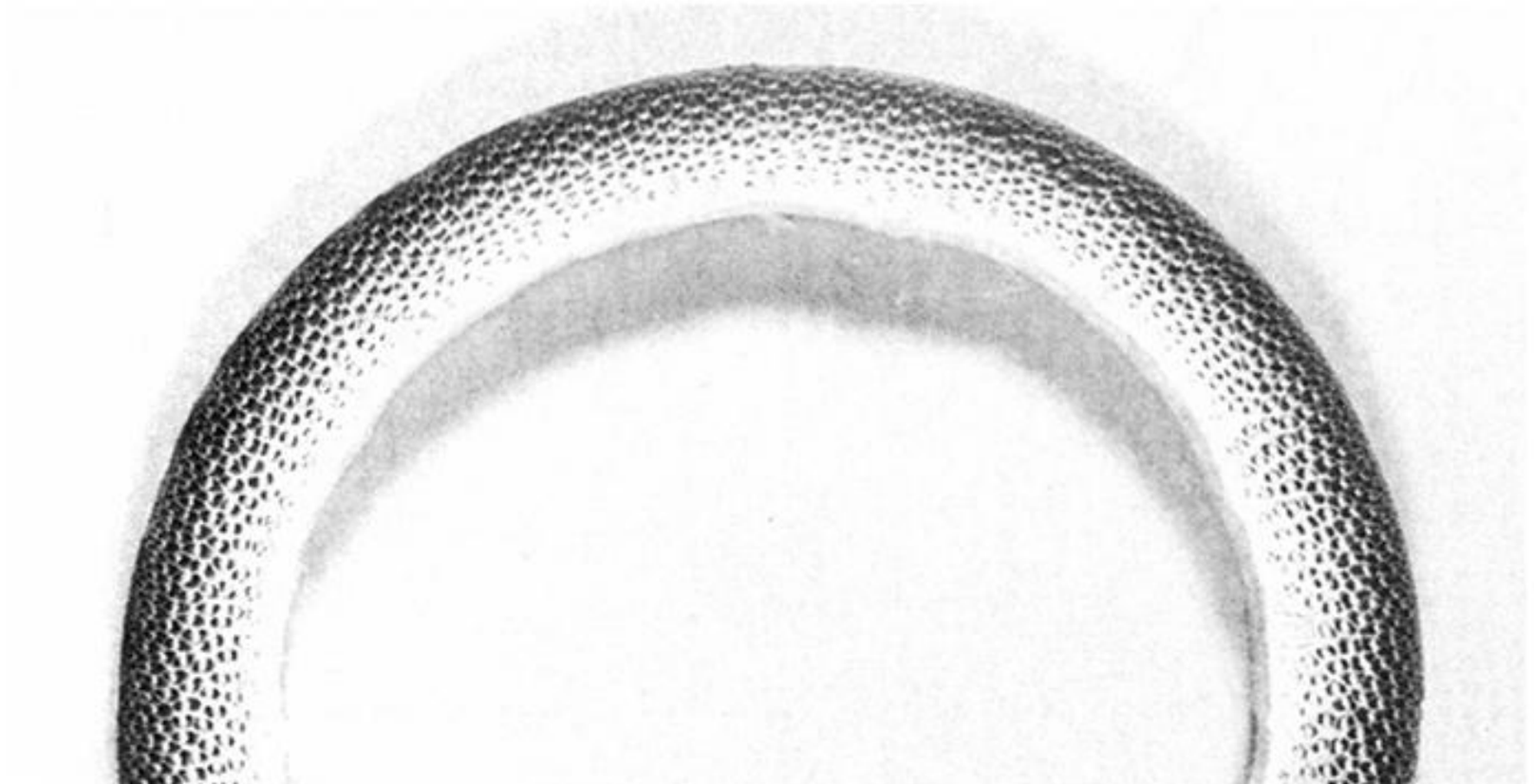

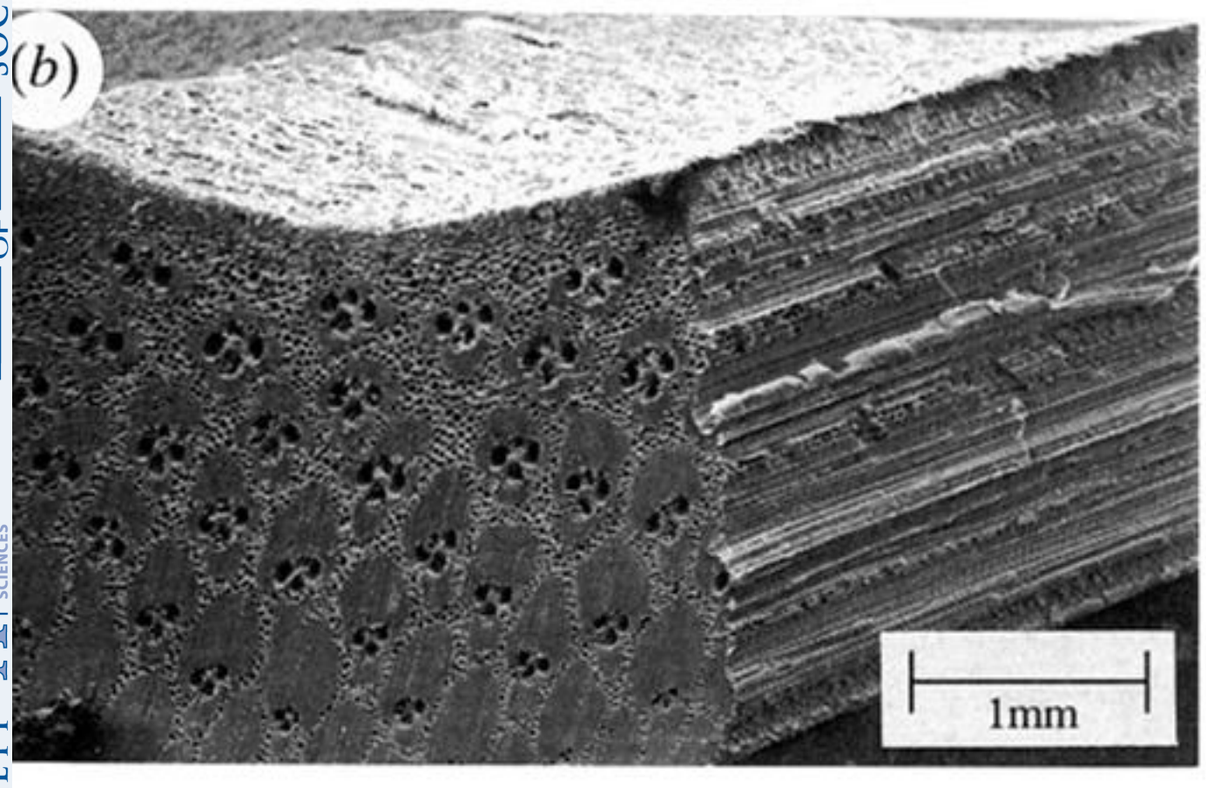

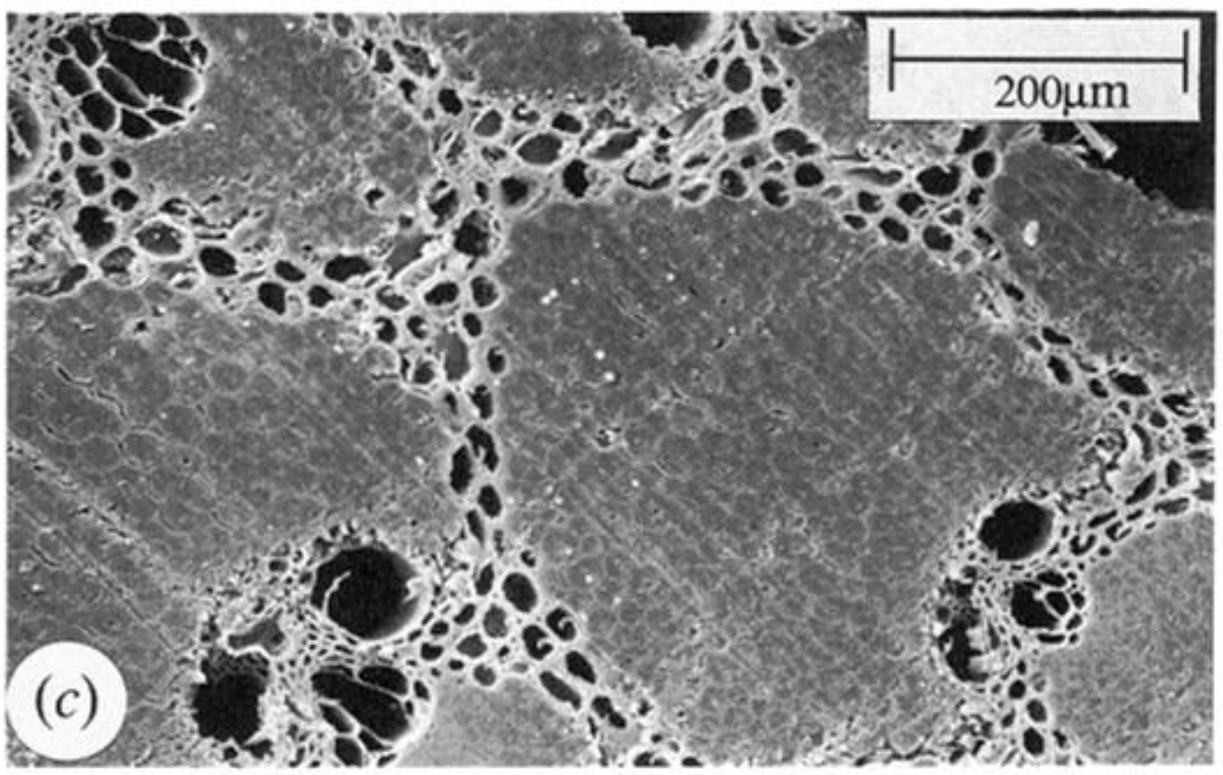

Figure 6. (*a*) Optical micrograph of a cross-section of a bamboo culm; (*b*) scanning electron micrograph of the wall of the bamboo culm showing the radial distribution of vascular bundles. The fibres and parenchyma are aligned with the longitudinal axis of the culm. The bundles have become almost totally sclerified in the tissue at the periphery. (*c*) Scanning electron micrograph of the vascular bundles at higher magnification.

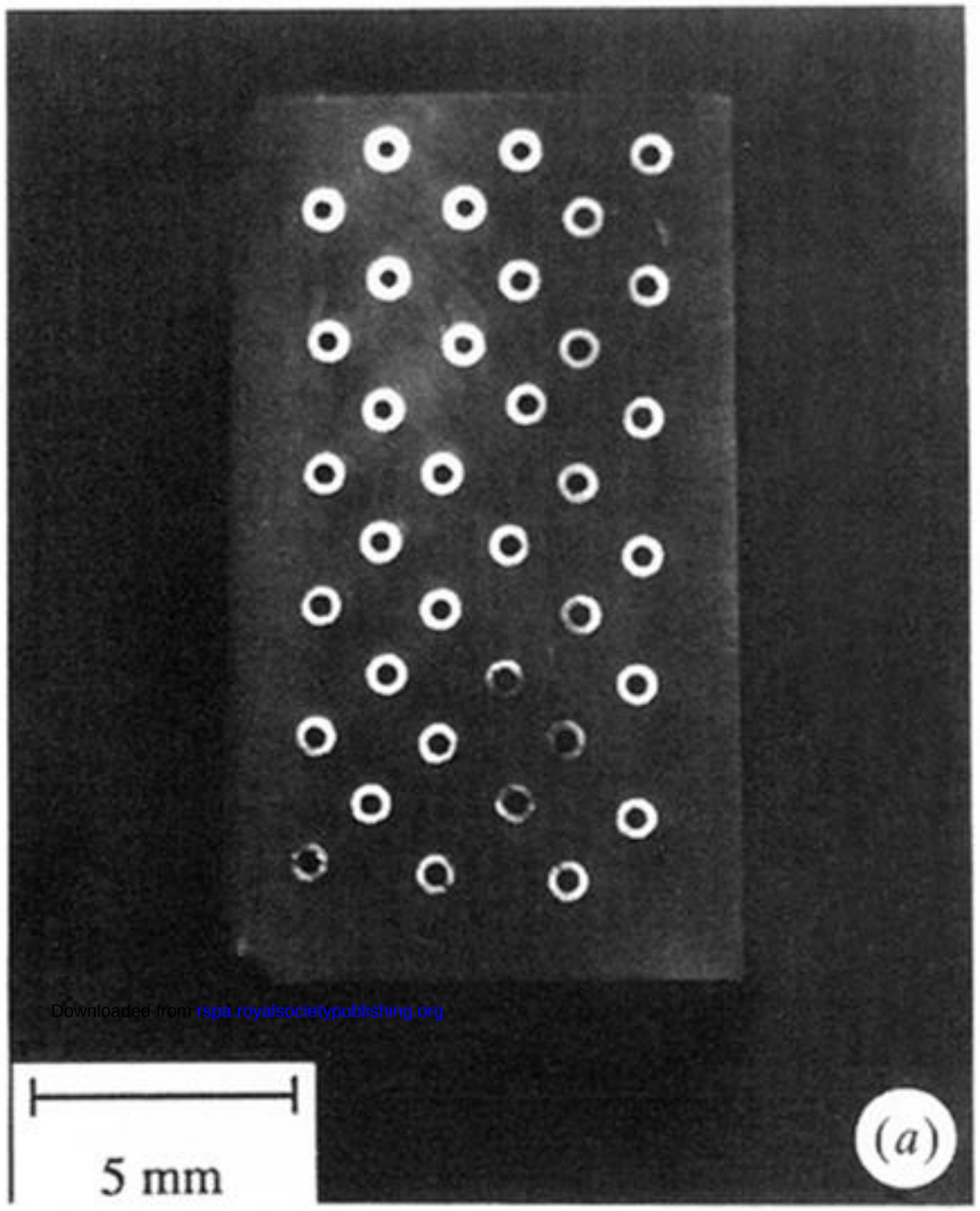

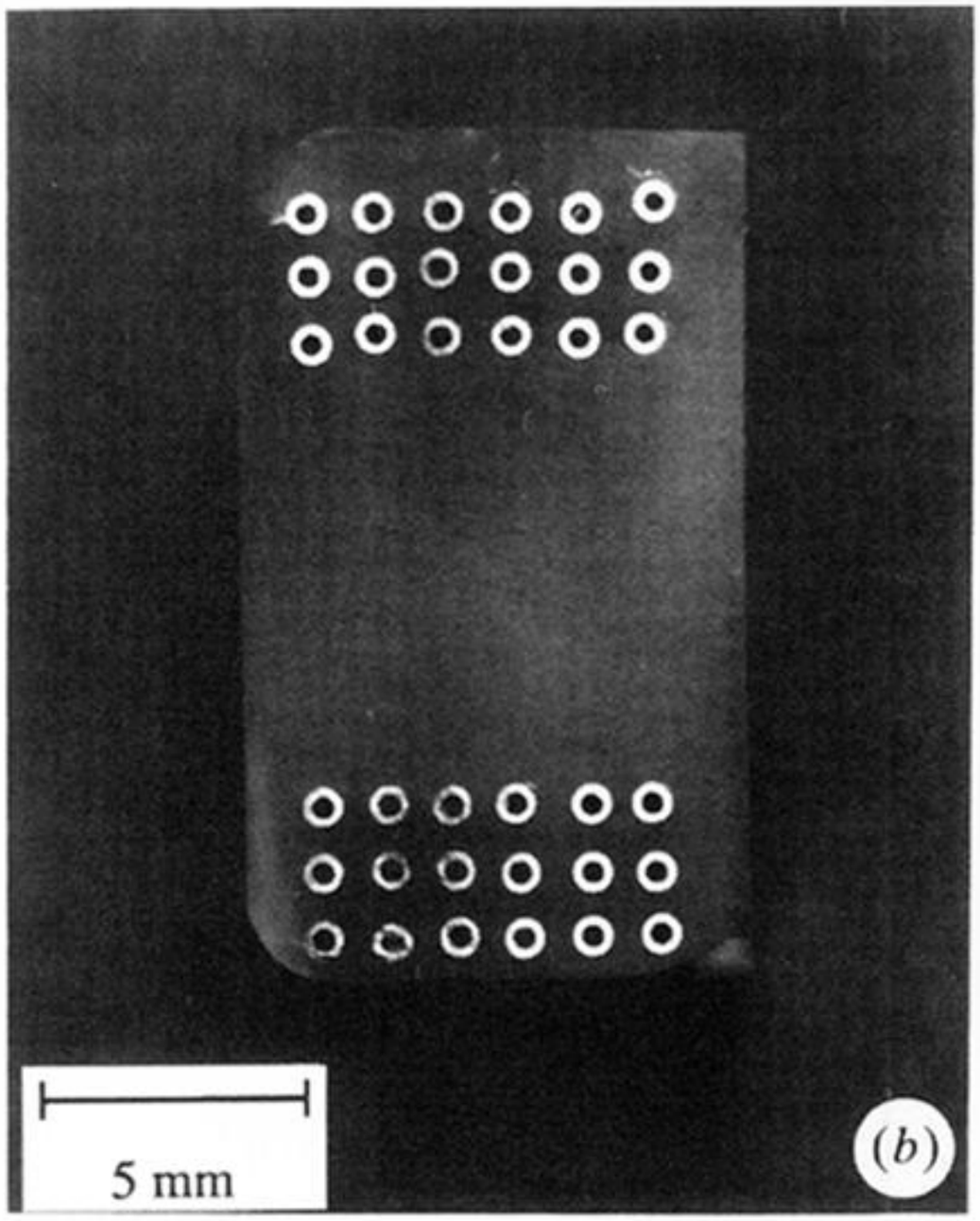

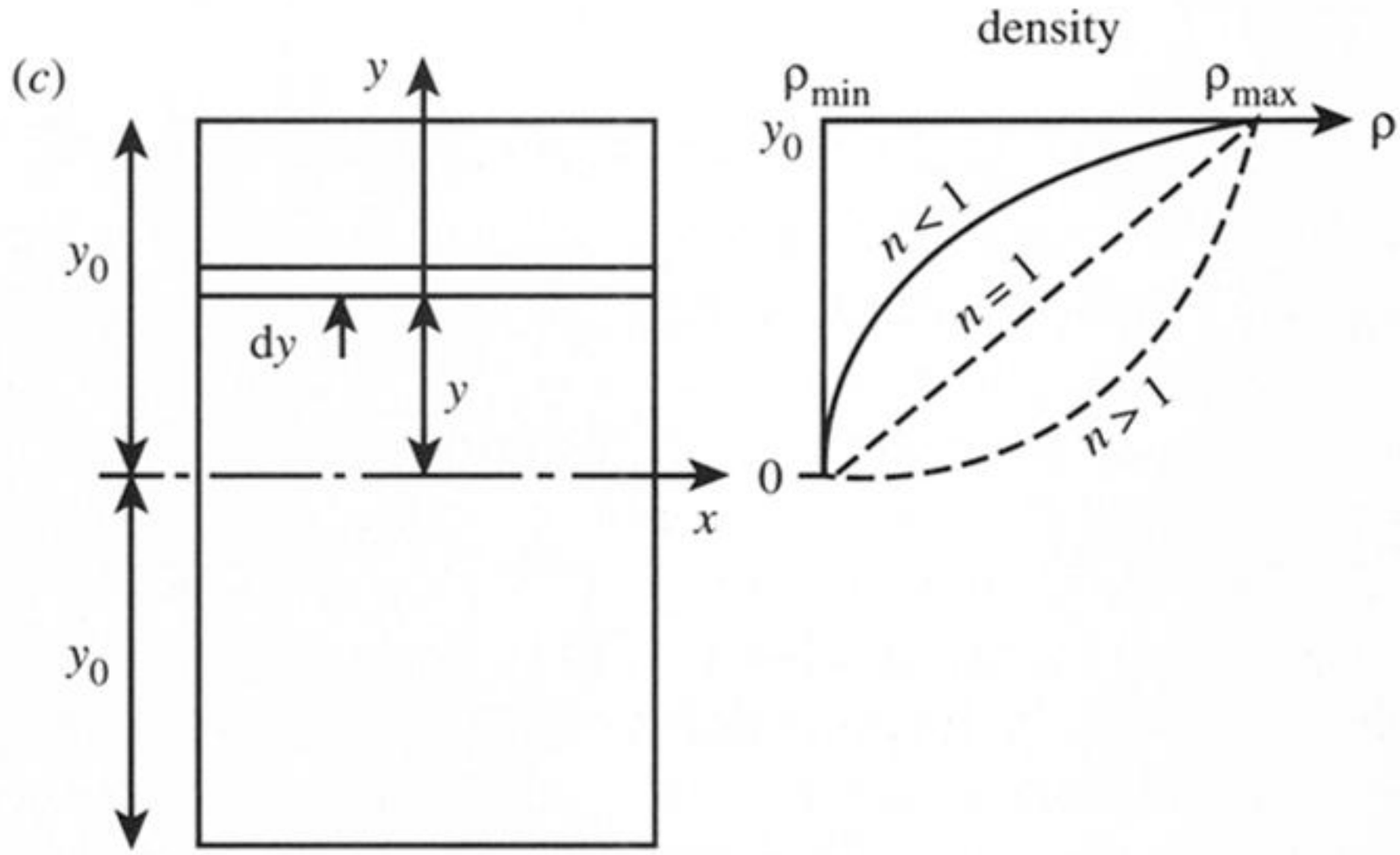

gure 10. Model materials with stainless steel tubes in an epoxy matrix: (*a*) uniform stribution of tubes; (*b*) tubes distributed in the depth direction only; (*c*) schematic a composite with a variation in the volume fraction of fibres in the depth direction $\rho(y) - \rho_{\min})/(\rho_{\max} - \rho_{\min}) = (y/y_0)^n$).

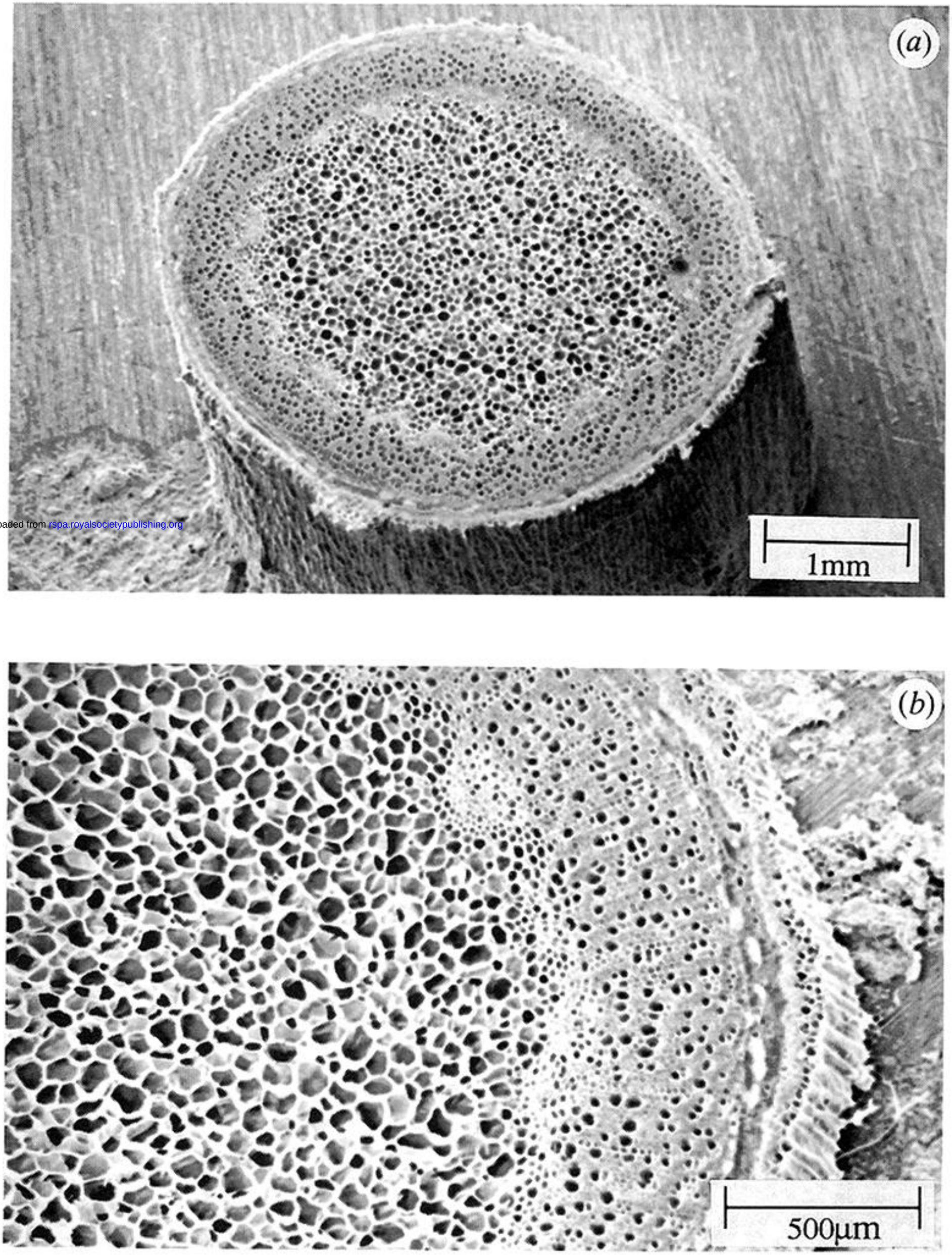

Figure 12. Scanning electron micrographs of hawthorn (*Craetagus*) showing the outer, almost fully dense, cylindrical shell with an inner layer of foam-like parenchyma cells.

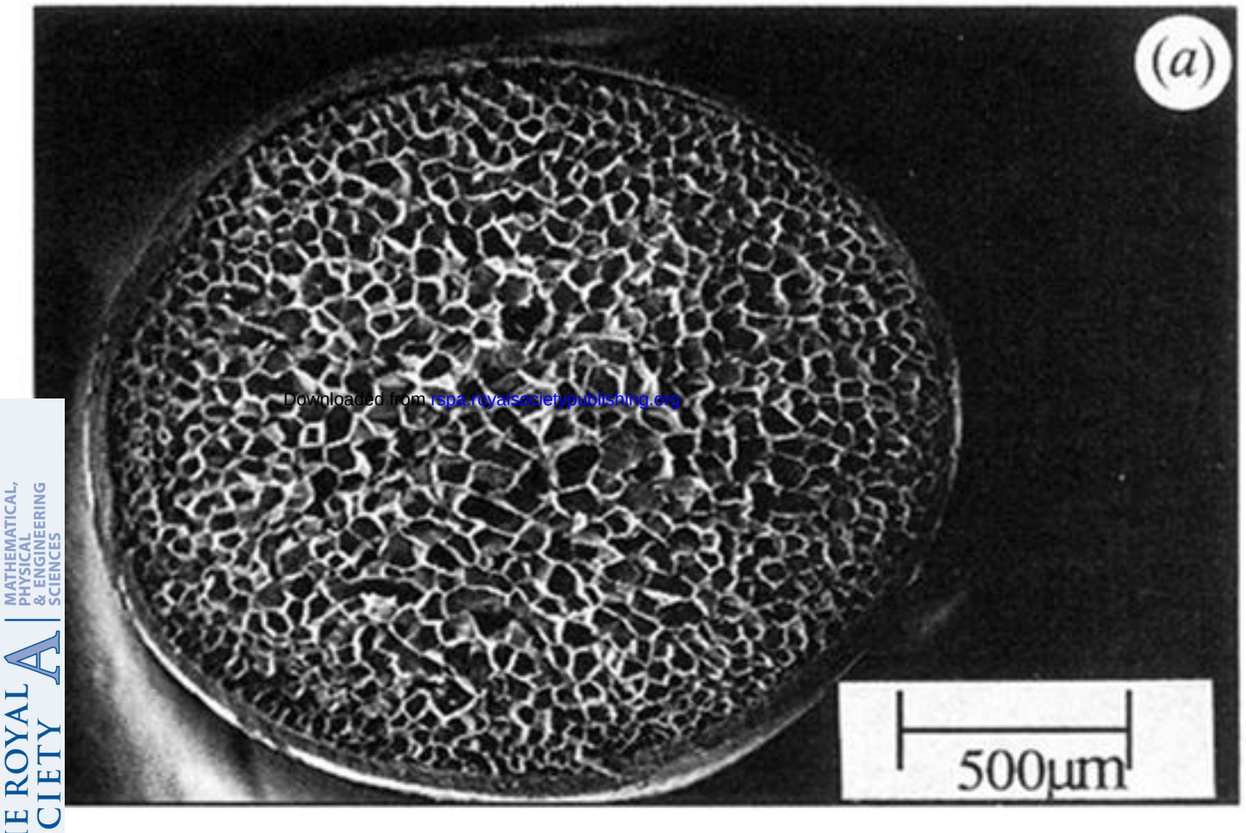

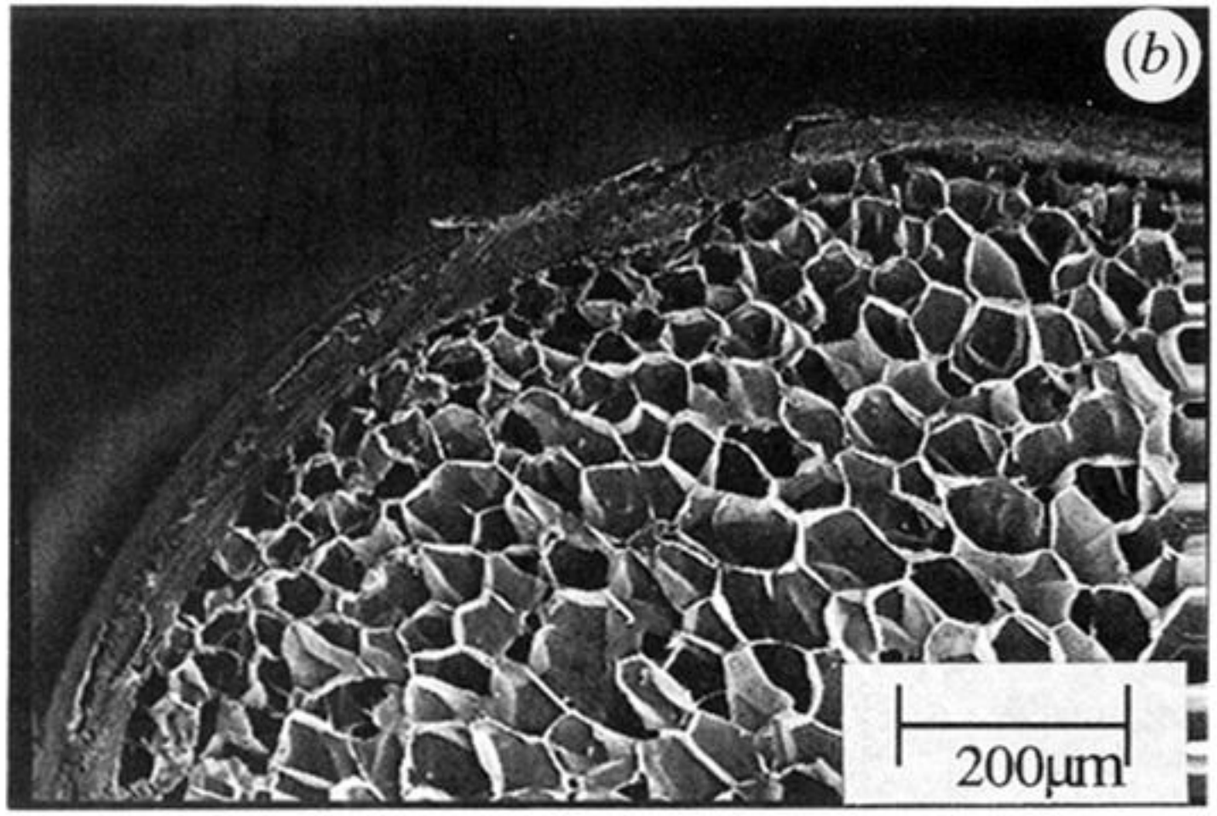

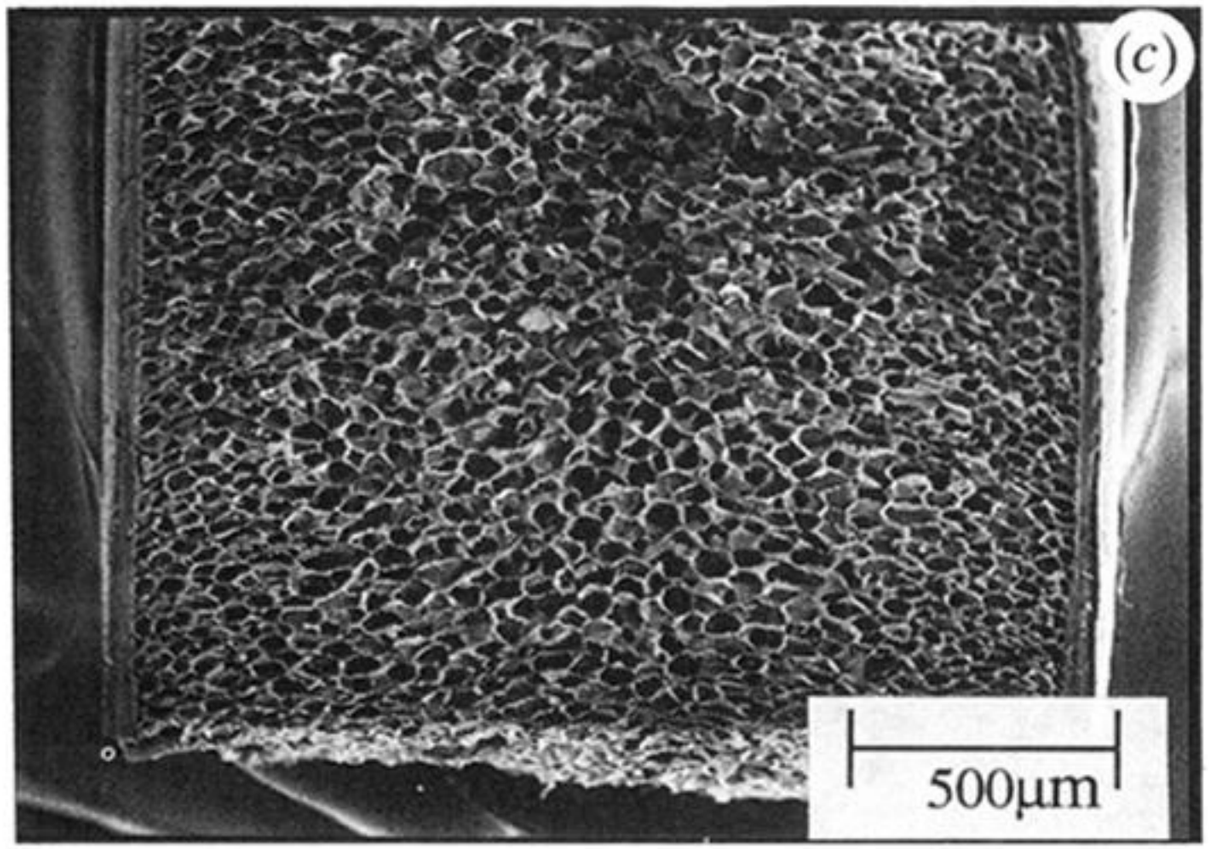

Figure 13. Scanning electron micrographs of porcupine (*Erethizon*) quills. (a, b) Transverse sections; (c) longitudinal section.